Numerical modelling of geomaterials at failure

Spetz, Alex

2019

Document Version:
Publisher's PDF, also known as Version of record

LUNDS UNIVERSITET

NUMERICAL MODELLING OF GEOMATERIALS AT FAILURE

ALEX SPETZ

Geotechnical Engineering

Doctoral Thesis

DEPARTMENT OF CONSTRUCTION SCIENCES

GEOTECHNICAL ENGINEERING

ISRN LUTVDG/TVGT--19/1016--SE (1-155) | ISSN 0349-4977 ISBN
978-91-7895-288-5 (print) | ISBN 978-91-7895-289-2 (pdf)
DOCTORAL THESIS

NUMERICAL MODELLING OF GEOMATERIALS AT FAILURE

ALEX SPETZ

Printed by Media-Tryck LU, Lund, Sweden, September 2019 *(Pl).*

For information, address:
Geotechnical Engineering, Dept. of Construction Sciences,
Faculty of Engineering LTH, Lund University, Box 118, SE-221 00 Lund, Sweden.
Homepage: www.geoteknik.lth.se

Acknowledgements

This dissertation was carried out at the Department of Construction Sciences at Faculty of Engineering, LTH at Lund University. This work was financially supported by the Development Fund of the Swedish Construction Industry, SBUF. The support is gratefully acknowledged.

First I would like to thank my supervisors professor Ola Dahlblom, Erika Tudisco and Ralf Denzer, at the Department of Construction Science and Per Lindh, at the Swedish Geotechnical Institute, SGI, for their support, patience and encouragement. I would also like to thank the staff of the Department of Construction Sciences and the fellow graduate students, with a special thanks to Erik Serrano for his sensitivity and understanding. Thanks to Bo Zadig for technical help and with the design of the cover for the thesis. I would like to give special thanks to Vedad, Daniel, Nikolaos and Philip, whom I sheared office with, you all helped with brightening my days with interesting discussions.

I would also like to give a kind thank Tuong Lam Nguyen, Gioacchino Viggiani, Pierre Vacher and Stephen Hall for providing the experimental results produced at Laboratoire 3SR, Grenoble, France. Furthermore, I would like to thank the staff at the Swedish National Infrastructure for Computing (SNIC) at LUNARC, the Center for Scientific and Technical Computing at Lund University for technical support during this work.

I would also like to express my gratitude and love to my parents, Charlie and Solveig for their endless support during my entire education and life in general. I would like to thank my brother for being a great support in difficult times. Finally I would like to thank Theresia for brightening up my days.

Lund, August 2019
Alex Spetz

Abstract

Geotechnical engineering is the science dealing with mechanics of soils and rocks and its engineering applications. Geotechnical engineering projects vary in a wide range, from evaluation of the stability of natural slopes and man-made soil deposits, to the design of earthworks and foundations. Traditional methods, using manual calculations or simplified computational methods, do not, as a rule, take into account the effects of soil-structure interaction, which can have a significant impact on the behaviour of the structure. The aim of the research presented in this dissertation is focussed on developing methods to analyse soil and rock behaviour. The research is in one part concerned with how soil-structure interaction can affect the design of foundations and geotechnical structures. The second part of the work is focussed on developing new methods to model geotechnical applications.

When designing foundations it is a common practice that separate numerical models are used in the analysis of soil behaviour and of structural behaviour. A common procedure is that the geotechnical engineer establishes a model of the site conditions and performs a simulation of the behaviour of the ground using pre calculated load values received from the structural engineer. The resulting settlements can then in turn be used in the dimensioning of the structure. Using separate models can lead to unrealistic prediction of the behaviour of both structure and load, as the soil-structure interactions are disregarded. As the use of computational methods is increasing, both to simulate the response in soil and during the structural design. Paper A enlightens some of the risk that misuse of simplifications can lead to. The paper includes an evaluation of how using the modulus of subgrade reaction during the design of foundations can affect the dimensioning of the reinforcements in shallow foundations.

Isogeometric analysis, is a numerical method that uses non-uniform rational B-splines (NURBS) as basis functions instead of the Lagrangian polynomials often used in the finite element method. These functions have a higher-order of continuity, making it possible to represent complex geometries exactly. The Higher-order continuity of the basis functions is also beneficial for problems that include frictional sliding and large displacements, overcoming the numerical instability caused by the C^0-continuous basis functions often used in finite element formulations. A common problem in many geotechnical simulations. Paper B presents numerical simulations of soil plasticity using isogeometric analysis comparing the results to the solutions from conventional finite element method.

The ability to predict rock behaviour using numerical models is pivotal to solve many rock-engineering problems. Numerical modelling can also be used to improve our understanding of the complicated failure process in rock. With models that better capture the fundamental failure mechanisms observed in laboratory, our ability

to generate reliable large-scale models improves. Prediction of brittle fractures in rock and soil is a complex problem with a number of active research areas, ranging from landslides and fault mechanics to hydraulic fracturing.

In this work a modified phase-field fracture model that can predict crack nucleation in porous rock and rock-like material is presented. In porous rock, the critical release rate for tensile cracks can be orders of magnitude smaller than the critical energy release rate for shear cracks and compressive stresses can lead to the formation of compaction driven cracks. Paper C and Paper D demonstrates the capability of the proposed phase-field model for simulating the evolution of mixed mode fractures and compressive driven fractures in porous artificial rocks and Neapolitan Fine Grained Tuff.

Populärvetenskaplig sammanfattning

Alla anläggningsprojekt, vare sig det gäller en bro, tunnel eller byggnad, har gemensamt att konstruktionen måste stödjas av den underliggande och omgivande marken. Konstruktionens egentyngd och eventuella yttre laster kommer att överföras till den underliggande och omgivande marken. Det är därför viktigt att kunna förutsäga eventuell rörelse eller brott i marken vid utformningen av varje ny konstruktion. För enklare konstruktioner kan dessa beräkningar ofta utföras med förenklade metoder eller handberäkningar. Vid större byggnadsprojekt eller vid komplicerade markförhållanden krävs däremot ofta numeriska beräkningsmetoder. En stor fördel med numeriska simuleringar är att flera olika alternativ kan testas på hela konstruktionen innan slutgiltiga designbeslut tas, vilket kan innebära besparingar i både design- och produktionsledet. Vidare finns möjlighet att snabbt förändra designen om förutsättningarna blir förändrade, eller om det under produktion visar sig att andra grundförhållanden skiljer sig från de förhållanden som man har utgått från vid projekteringen. När det gäller komplicerade anläggningsprojekt används numeriska beräkningsmetoder både i grundläggningsdimensioneringen och i betong- eller ståldimensioneringen. I det arbete som presenteras i den här avhandlingen har olika typer av numeriska metoder för simulering av geotekniska tillämpningar undersökts. Ett vanligt förfarande är att geotekniker skapar en teoretisk modell av grundläggningsförhållandena och gör beräkningar baserade på laster som har tagits fram av konstruktören. Resultaten från geoteknikerns beräkningar används sedan av konstruktören vid dimensionering av konstruktionen. Vid numeriska simuleringar för konstruktioner där det är av stor vikt att interaktionen mellan jord och konstruktion modelleras på ett realistiskt sätt är en gemensam modell ett bättre tillvägagångssätt.

I den första delen av det här arbetet undersöks hur användningen av separata modeller kan påverka resultaten vid numeriska simuleringar av geotekniska konstruktioner. En metod som undersöks är att använda isogeometrisk analys för simulering av jord, en numerisk metod som har gett goda resultat för analys av kontakt mellan två ytor som utsätts för stora relativa deformationer med samtidig glidning, ett område som ofta leder till numerisk instabilitet med den metod som oftast används för numeriska simuleringar idag.

Vid belastning av så kallade duktila material, t.ex. segt stål, uppkommer synliga deformationer innan sprickor bildas. I spröda material däremot, t.ex. sten, sker ofta sprickbildning utan någon synlig varning, där sprickorna dessutom kan växa i mycket höga hastigheter. I den andra delen av det här arbetet behandlas sprickor i porösa bergarter. På grund av komplexiteten i sprickprocesserna spelar numeriska metoder och högpresterande datorer en avgörande roll i modern brottmekanik. När

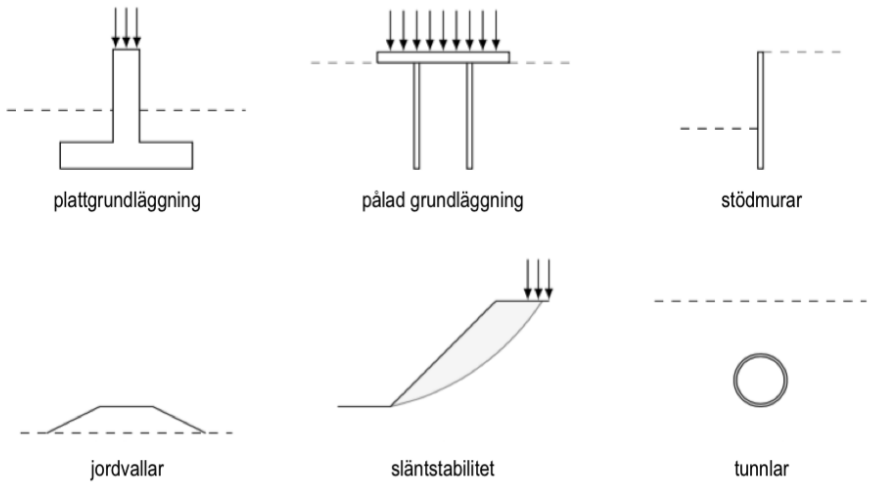

Figur 1: Exempel på geotekniska konstruktioner.

en spricka utvecklas uppstår det förändringar i objektets geometri, vilket konventionellt leder till att en ny geometri måste modelleras för varje förändring i sprickan, med långa beräkningstider som följd. Nyligen har alternativa metoder för numerisk simulering av spröda brott utvecklats. I de nya metoderna approximeras sprickorna av ett så kallat phase-field, vilket jämnar ut sprickans gräns över ett litet område och inga diskontinuiteter införs i beräkningsmodellen. I det här arbetet har en numerisk metod för simulering av spröda brott vidareutvecklats och tillämpats för simuleringar av sprickor i sten och stenliknande material. Denna metod leder till ett antal fördelar jämfört med konventionell brottmekanik, eftersom implementeringen inte kräver att sprickytorna spåras och modelleras när en spricka utvecklas.

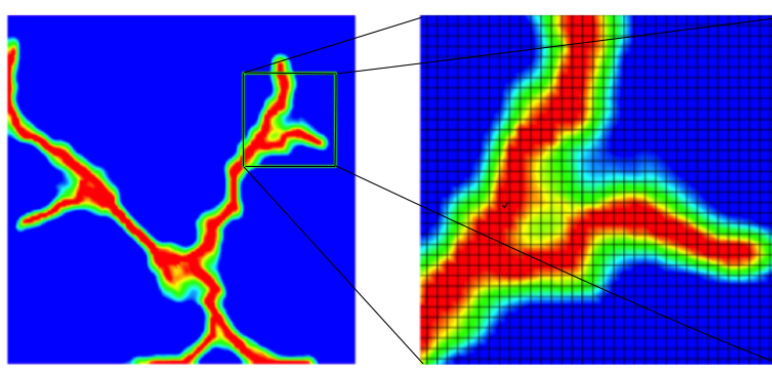

Figur 2: Genom att approximera en spricka med ett phase-field kan geometrin vara konstant genom hela simuleringen.

Contents

Part I

Introduction and overview

1 Introduction

All civil engineering projects, whether a bridge, tunnel or building, have in common that the structure has to be supported by the underlying and surrounding soil or rock. The weight and loads applied to the structure will be transferred to the underlying and surrounding material. It is therefore essential to predict any potential movement or failure of the underlying material as a part of the design of any new structure. Consequently, it is also important to assess how any movement in the underlying material affects the structure itself. Understanding the behaviour of geomaterials (e.g., clay, sand, gravel, or rock) and their interaction with structures is therefore important for a realistic and economic analysis of all civil engineering projects. Here, it is in place to state, that, for the remainder of this work, Geotechnical engineering is the branch of civil engineering concerned with construction built on or surrounded by the ground, whereas Geomechanics is the science in which the mechanical behaviour of soil and rock under loading is studied.

In contrast to other construction materials, geo-materials are natural materials. Hence, the material properties are not selected by an engineer but predetermined by the location of the structure, and it is therefore important to have deep understanding of how different soils and rocks behave under loading. Soil and rock are natural materials with properties that distinguish them from other construction materials, and even though soils in general consist of rock that has been weathered into smaller particles over time there are important differences between them. Soils and rocks are multiphase materials, consisting of solid particles with intermediate pores filled with air or water, where the size and shape of the grains can vary form a couple of millimetres in sand to less than 2 μm in clayey soils. Whereas, most rock consists of a composition of crystals and amorphous particles bonded with varying amounts of cementing material. The chemical composition of the crystals may be relatively homogeneous, as in some limestone, or very heterogeneous, as in granite. The size of the crystals may also vary both in size and distribution, of a typical size no greater than a few centimetres. Due to these similarities between soil and rock, at one end of the spectrum, rock mechanics grades into soil mechanics and at the other end, at great depths, rock mechanics grades into the mechanical aspects of structural geology. In turn, the behaviour of a soil can vary greatly depending on

the size and the shape of the individual particles, the consolidation grade and the porosity.

This work focusses on two important aspects of geotechnical engineering: the use of numerical methods and the simulation of fracture propagation in rocks. The first two papers are focussed on how modern numerical methods can make a difference in the design procedure of geotechnical structures. When designing geotechnical constructions, the complicated properties of soil as construction materials often make advanced analysis necessary. The design of geotechnical problems often includes a number of complex physical aspects, ranging from highly non-linear stress-strain relations to pore-pressure variations. To overcome these difficulties, the use of numerical analysis, e.g., the finite element method (FEM), has become common practice in modern geotechnical engineering. The first paper is focussed on how the use or misuse of numerical methods might affect the design of rather simple foundations while the second paper explores the possibility of using isogeometric analysis to simulate soil behaviour. Another important aspect in geotechnical engineering is the ability to predict and realistically reproduce rock mass behaviour using numerical models. Numerical modelling can improve our understanding of the complicated failure process in rock and the many factors affecting the behaviour of fractured rock. When our models manage to better capture the fundamental failure mechanisms observed in laboratory, our ability to generate reliable large-scale models improves. In Paper C and Paper D an alternative method to simulate crack propagation in rock using a phase-field fracture model is presented.

1.1 AIMS AND OBJECTIVES

The original aim with this research was to develop methods to improve the design of foundations and geotechnical structures using advanced numerical methods, with a focus on how numerical methods can affect the design of geotechnical structures. In general, structural- and geotechnical engineers use separate models during the design procedure, which may lead to loss of synergy effects between structural elements and the underlying soil. Moreover, it is common practice to use simplifications, e.g., by idealising a soil as a series of independent springs to model soil-structure interaction. The aim with Paper A, was to quantify the effect of using simplified methods when designing simple foundations.

During the work with the Paper A it became obvious that, how the soil-structure interaction is modelled can have a large influence on the results and that commercial tools often use different methods and simplifications to model the soil-structure interaction. Even though soil-structure interaction can be modelled using a number of different techniques, too crude simplifications can lead to misconceptions. Moreover, geotechnical analyses often include soil-structure interaction problems

with friction and sliding, which can be difficult to analyse even using FEM, as the C^0-continuous basis functions commonly used can lead to numerical instability.

In recent years isogeometric analysis has shown promising results for complex contact problems. The purpose with Paper B was to investigate the effect of the higher order basis functions used in the isogeometric framework on simulations of soil behaviour. Even though the result presented in Paper B demonstrated that the isogeometric framework can be used to simulate soil behaviour and plastic deformation, it also showed that the work with implementing both a realistic soil plasticity model and a modern contact algorithm would be a too great a commitment for the scope of this work.

Paper C and Paper D focus on another important aspect in geotechnical engineering, the ability to predict and realistically reproduce failure in rock. In recent times, phase-field fracture models have been introduced as an alternative method for numerical simulations of brittle fractures. The method has been used with success in a number of fields, including dynamic fracture mechanics [1–3], coupled thermo-mechanical-driven fractures [4], and high-order phase-field approaches [5], to name a few. However, these contributions assume that the critical energy release rate for different fracture modes are equal, which is not the case for rocks and rock like materials, see e.g., [6]. The aim of the work that resulted in Paper C and Paper D was to present a modified phase-field fracture model that distinguishes fractures in Mode I and Mode II as well as fractures driven by compressive stresses.

1.2 DISPOSITION

This thesis consists of two parts, where the first part is an overview of the work divided in six chapters. The second part consists of four appended papers produced during this work.

The chapters of the first part of this thesis are organised as follows. Chapter 1 gives an introduction to the thesis, stating the aims and objectives of this work. Chapter 2 gives a summary of the appended papers. Chapter 3 gives a brief introduction to geotechnical engineering. Chapter 4 introduces the theoretical framework of soil and rock mechanics. Chapter 5 gives an overview of the theories and numerical methods used to simulate soil and rock behaviour in this work. Chapter 6 concludes the thesis.

2 Summary of appended papers

Paper A

Paper A presents an evaluation on how using the modulus of subgrade reaction during the design of foundation can effect the dimensioning of the reinforcements in shallow foundations. To investigate how common misconceptions can affect the design, numerical studies using the modulus of subgrade reaction to idealise the behaviour of the underlying soil have been compared to full finite element analysis. To evaluate the reinforcement needs in the foundation, the advanced three-layer model described in [7], have been implemented and used within a general purpose FE-tool.

The paper concludes that it is important to have a good understanding of the concept behind the modulus of subgrade reactions, if it is to be used to design the reinforcements in concrete slabs. It also concludes, that using an incorrect value of the subgrade modulus, k_s, can lead to erroneous dimensioning of the reinforcement.

Contributions by Alex Spetz

Alex was the main author of the paper, implemented the method and carried out all the simulations using Comsol Multiphysics and MATLAB as well as drawing the main conclusions.

Paper B

Paper B presents numerical simulations of soil plasticity using isogeometric analysis. The results from the isogeometric analysis is compared to conventional finite element analysis, to evaluate the effects of using higher-order basis-functions of for simulation of soil plasticity. The paper gives a brief outline of the theory behind the isogeometric concept. The paper includes a presentation of the Drucker-Prager criterion, which is used to simulate the soil behaviour in this work. The paper

concludes with numerical examples in two- and three-dimensions, which assess the accuracy of isogeometric analysis for simulations of soil behavior. The numerical examples presented show that, for drained soils, the results from isogeometric analysis are overall in good agreement with the conventional finite element method in two- and three-dimensions.

Contributions by Alex Spetz

Alex was the main author of the paper, planned the research and implemented the isogeometric framework and the material model in FORTRAN as well as carrying out the reference simulations using Comsol Multiphysics.

Paper C

In Paper C a modified phase-field fracture model for simulation of crack propagation in porous rocks is proposed. The presented model introduces a split of the fracture energy release rate to capture the characteristic behaviour of fractures in porous rock. In porous rock, the critical release rate for tensile cracks can be orders of magnitude smaller than the energy release rate for shear cracks and compressive stresses can lead to the formation of compaction bands. To capture these characteristic behaviours we have introduced a split of the fracture energy release rate into three components. To demonstrate the capability of the modified phase-field fracture model first introduced in this work, we have compared the numerical results to experimental observations performed on rock samples subjected to uniaxial plane strain compression. The presented comparison shows that the modified phase-field fracture model gives results in good agreement to the experimental observations both with respect to crack patterns and critical stress loads. It has also been shown that the proposed phase-field model is able to reproduce the formation of compaction bands as well as complex crack patterns without any additional algorithmic treatment.

Contributions by Alex Spetz

Alex was the main author of the paper, developed and implemented the method and carried out the numerical simulations, as well as being a large contributor to the drawn conclusions.

Paper D

Paper D suggests a modified phase-field model for simulating the evolution of mixed mode fractures and compressive driven fractures in both a porous artificial rock and in Neapolitan Fine Grained Tuff. The numerical model has been calibrated using experimental observations of rock samples with a single saw cut under uniaxial plane strain compression. For the purpose of validation, results from the numerical model are compared to Meuwissen samples with different angles of rock bridge inclination subjected to uniaxial compression. The simulated results are compared to experimental data, both qualitatively and quantitatively. It is shown that the proposed model is able to capture the emergence of shear cracks between the notches observed in the Neapolitan Fine Grained Tuff samples as well as the propagation pattern of cracks driven by compressive stresses observed in the artificial rock samples. Additionally, the typical types of complex crack patterns observed in experimental tests are successfully reproduced, as well as the critical loads.

Contributions by Alex Spetz

Alex was the main author of the paper, took part in the planning of the paper and developed and implemented the method as well as carried out the numerical simulations, as well as being a large contributor to the drawn conclusions.

3 Geotechnical engineering

Geotechnical engineering is the science dealing with mechanics of soils and rocks and its engineering applications. Geotechnical engineering projects vary in a wide range, from evaluation of the stability of natural slopes and man-made soil deposits, to design of earthworks and foundations. Figure 3.1 illustrates some examples of geotechnical structures. Research within the field ranges from analytical and numerical studies of geotechnical problems to constitutive modelling, experimental modelling and design. The work of geotechnical engineers plays an important role in all civil engineering projects built on or in the ground, and is vital during evaluation of natural hazards such as earthquakes, liquefaction, sinkholes and landslides. This chapter starts with a historical overview and introduction to geotechnical engineering and is continued by an introduction to the design objectives and requirements for geotechnical analysis.

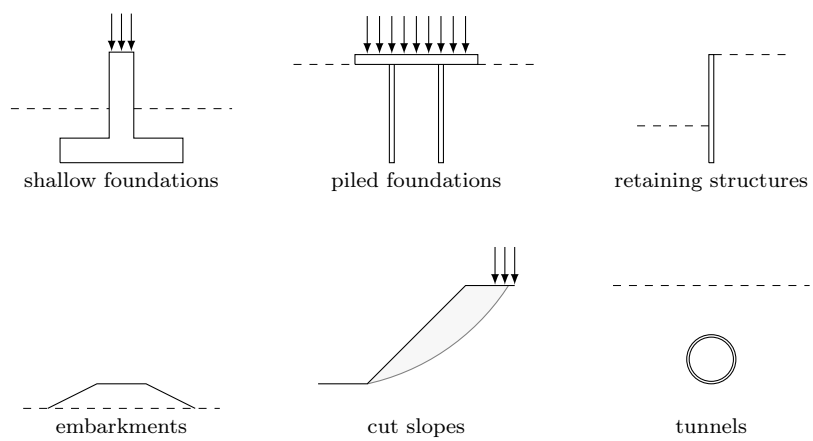

Figure 3.1: Examples of geotechnical structures.

3.1 BACKGROUND

Historically, geotechnical engineering was applied by trial and error or observational experience. Problems like the notorious leaning tower of Pisa motivated engineers to take a more scientific approach to geotechnical engineering. The first documented theories in soil mechanics where presented by Charles Augustin de Coulomb to the Academy of Science in Paris, year 1773. The theory regarded active and passive earth pressure and was published three years later, entitled "Essai sur une application des régles des maximis et minimis à quelques problémes de statique relatifs à l'architecture", the theory remains in use even to this day in basic engineering practice. During the eighteenth and nineteenth century a series of key discoveries in fundamental soil-mechanics and flow through porous media were published by Coulomb, Rankine, Darcy, Mohr and Atterberg. Karl von Terzaghi, an Austrian engineer, is often regarded as the father of modern soil mechanics and considered to have been the first person to achieve an engineering understanding of soil as an engineering material, with properties that can be measured in standardised ways. In his work "Erdbaumechanik" published in 1924, he presented his theory of consolidation and the effective stress, which revolutionised the field of geotechnical engineering, suggesting that the deformations in a soil are governed by the effective stresses [8].

The increased knowledge of soil behaviour led to development of approximate methods for solving a number of engineering problems. However, these approximate or simplified methods do not provide sufficient solutions for the complexities of many geotechnical problems. Much progress has been made in the development of constitutive models, where early work led to the development of the Mohr-Coulomb criterion, developed from Charles Augustin de Coulomb's work concerning shear failure in soils and from Christian Otto Mohr's work regarding Mohr's circle. The criterion is a rather crude simplification of soil's behaviour. Even though it represents the failure for drained conditions rather well, the effective stress path that is followed in un-drained materials may deviate significantly from observations [9]. In 1952, Drucker and Prager presented the Drucker-Prager criterion which can be seen as a generalisation of the Mohr-Coulomb criterion that accounts for the effects from all principal stresses [10]. The Drucker-Prager criterion takes the shape of a circle when viewed in the deviator plane, as opposite to the Mohr-Coulomb criterion which presents sharp corners. This makes the Drucker-Prager criterion more stable in numerical calculations than the Mohr-Coulomb criterion at the cost of being a cruder representation of soil behaviour.

To overcome the weaknesses posted by the Mohr-Coulomb and Drucker-Prager criteria, researchers have investigated the possibility of modelling soil as a strain-hardening material. The soil mechanics group at Cambridge University made significant contributions to the work around these strain-hardening models, referred

to as critical-state models, [11]. The research led by Professor Sir Alec Skempton at the Imperial Geotechnical Laboratories, led to the formulation of the Cam-Clay model, Roscoe et al. [12]. Professor John Burland suggested a modification of the model, which subsequently led to the Modified Cam-Clay model presented in [13]. Although the Cam-Clay models achieve better predictions compared to observed soil behaviour than the Mohr-Coulomb and Drucker-Prager models, the model is limited when modelling frictional materials and fail to predict observed softening and dilatancy of dense sands and undrained response of very loose sands [14].

Compared to the field of soil mechanics, the development of rock mechanics has been much slower, and until the middle of the 20th century rock mechanics was a branch of soil mechanics. Unfortunately, accidents have been a major contributing factor to the advancement of rock mechanics, where two major disasters in Europe stand out as the triggering factor for the creation of the International Society for Rock Mechanics. In December of 1959 the Malpasset dam, in southern France, burst. The cause of the disaster is foremost attributed to an inadequate geological survey. Geological investigations performed after the dam's collapse showed that it had been constructed on gneiss, an impermeable rock. The survey also found a fault in the bedrock just downstream of the dam. When the water level in the dam increased due to heavy rainfall the compressive forces in the foundation led to an increased permeability of the bedrock. This in turn led to uplift pressure at the left abutment, which is believed to have been the main cause of the dam failure. The second accident occurred a few years later in Vojant, Italy, where in October 1963 a major rockslide into the dam lake caused a 250 metres tsunami. The tsunami led to the complete destruction of several villages and towns, and close to two thousand dead. With increased efforts to get a better understanding of rock behaviour, the field of rock mechanics has made great advancements during the past decades.

As rock mechanics historically is closely related to soil mechanics, the Mohr-Coulomb criterion is a common model used also for analysis of rock. However, experimental data showed a much larger ratio of the compressive to tensile strength than predicted by the Mohr-Coulomb criterion. During the the years numerous mathematical models based on the Mohr-Coulomb criterion have been proposed to overcome this issue. However, rock masses are in general broken up by joints and faults containing pressurised fluids, which is not accounted for in Mohr-Coulomb based models. In 1980, Evert Hoek and E. T. Brown presented the original version of their widely used failure criterion, which is capable of fitting data from many different rocks. The Hoek-Brown failure criterion is an empirical failure criterion with the basic idea that the behaviour of rocks can be captured by reducing the mechanical properties of an intact rock by adding correctional coefficiants. These correctional coefficions may be due to the existence of joints and faults in the rock mass [15]. With an increased capability of predicting failure in rock, the number of engineering projects involving rock has increased, either as construction material or as foundation. As the field has grown, today rock-mechanics is an interdisciplinary

field, ranging from engineering geology and hydraulics to fracture mechanics and physics.

The development of numerical methods for geotechnical applications is placing new demands on the geotechnical engineers. To perform good numerical analysis it is essential to have an understanding of the constitutive model applied and its shortcomings along with a sound knowledge of the governing design objectives.

3.2 DESIGN OBJECTIVES AND REQUIREMENTS

The first requirement when designing a geotechnical structure is to determine ground conditions. Since the material properties of soil and rock vary with both location and depth, almost all major civil engineering projects start with field investigations from which the layering and properties of the ground are determined, as well as the position of the ground water table. The resulting stratigraphy of the subsurface can then be used in the design. To have a good stratigraphic model of the ground conditions is essential in the design of geotechnical structures. For example, when designing a new foundation, a ground layer model is used to ensure that the foundation can withstand any man made and natural loads, vertical and lateral pressures from strong winds or earthquakes as well as the weight of the building itself. Design objectives vary depending on the type of structure that is designed. It is, however, essential to ensure stability for all geotechnical structures. Figure 3.2 illustrates some of the design objectives for a spread footing [16]. In urban areas, the governing design requirement is often ensuring that the structure does not initiate movements in the soil that affect existing buildings and services. In addition, it is necessary to assess if the construction might affect the groundwater table and its implication on nearby structures.

3.3 NUMERICAL ANALYSIS IN GEOTECHNICAL APPLICATIONS

Due to the complex non-linear mechanical behaviour of soils and rock, simple analytical methods often fail to describe how the ground and structures interact. The advancement of computers in recent decades has made it possible to develop models using realistic non-linear relations to describe these mechanical behaviours. In modern geomechanics, computational methods e.g., finite element analysis (FEA) or finite different analysis (FDA), are widely used to predict the behaviour of foundations, structures and soil bodies. One big advantage of using numerical methods is that one analysis can be used to study a large number of design objectives at the same time, e.g., movement in both soil and structure, variation of pore water

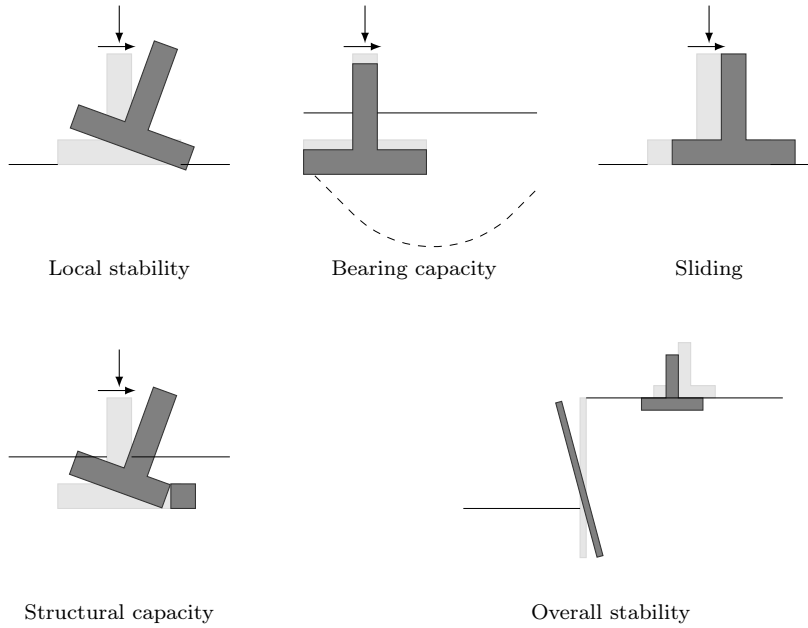

Figure 3.2: Design objectives for spread footings.

pressure as well as assessment of stresses and forces in the structural elements. Using manual calculations, these design objectives often require separate calculations. Another advantage of using numerical simulations is that various design options can be tested before final design decisions are made, which can result in economical savings. Furthermore, it is possible to quickly update a computer model and perform a new analysis. Another important aspect when modelling soils is the flexibility that a computer simulation brings during construction. If the ground conditions prove to be different during the construction than the preliminary survey indicated, an updated simulation can be conducted swiftly. When dealing with complex engineering projects, computational methods are often used both in the design of the foundation and in the design of the concrete or steel structure. Unfortunately, separate numerical models are often used to analyse soil behaviour and for design of the structure. A common procedure is that the geotechnical engineer establishes a model of the site conditions and performs a simulation of the behaviour of the ground using pre calculated load values received from the structural engineer. The resulting settlements can then in turn be used in the dimensioning of the structure. Using separate models can lead to unrealistic prediction of the behaviour of both structure and load, as the interactions between structural elements and soil is disregarded.

3.4 SOIL-STRUCTURE INTERACTION

For many geotechnical structures and foundations, relative motions occur between soil and structure. These relative motions at the interfaces can have a large influence on the overall behaviour of the system [17]. It is, therefore, important to incorporate the soil-structure interaction effects during the design. Examples of soil-structure interaction effects are illustrated in Figure 3.3. The figure shows a piled raft subjected to a spread load. The loading of the structure will give rise to stresses in the underlying and surrounding soil. Using manual calculations, the load on the structure is assumed to be transferred solitary through the piles to the surrounding soil. In reality, part of the load will be transferred directly from the raft to the underlying soil. Stress fields may also create arches between the structural components. Some of the methods that are used to simulate soil-structure interaction are discussed in the following.

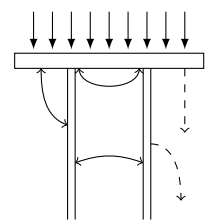

Figure 3.3: Soil structure interaction.

Spring idealisation

During the design of structural elements, a common method to model soil-structure interaction is to idealise the soil as a series of independent springs. The spring stiffness is often referred to as modulus of subgrade reaction and was first introduced by Winkler [18]. The original application was to compute the stresses and deformations in railroad structures. The method does, however, only give information on the structure, and gives no information on displacements or stress levels in the soil. Moreover, it can be difficult to determine the correct stiffness of the springs. The use of subgrade reactions during the design of foundations can therefore lead to misconceptions of the structural response. Figure 3.4 demonstrates the effect of using modulus of subgrade reaction for a raft foundation subjected to a spread load compared to a full numerical model. Comparing the predicted displacements and stress distribution, it becomes clear that the simplified method can lead to inefficient designs.

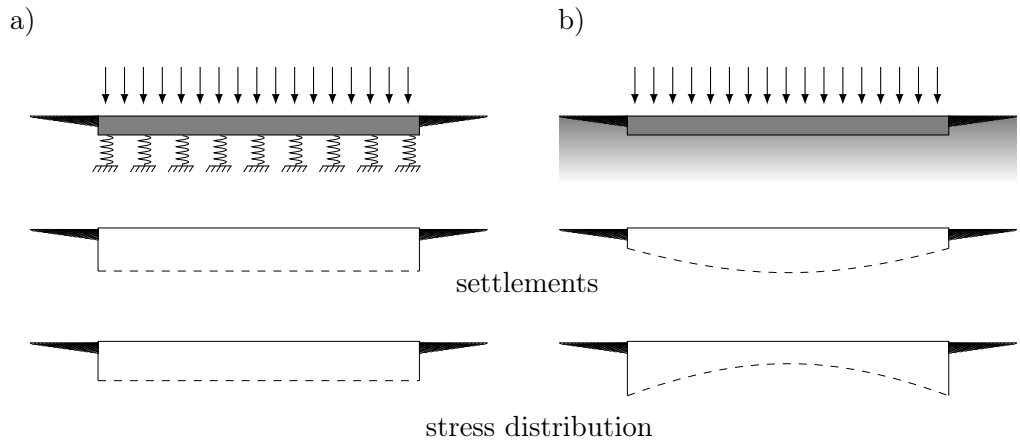

Figure 3.4: Illustration of predicted values, a) using springs to represent soil behaviour compared to, b) using a joint model that includes both the soil and structure.

Interface elements

Another method used to evaluate the effects of soil-structure interaction is to employ interface elements. These elements are placed in-between the soil and structure elements, simulating the behaviour in the soil close to the structure. The interface elements range from simple models that assume no relative motion to complex constitutive models. Interface elements were initially developed for rock joints, and typically use normal and tangential stiffness to model the pressure transfer and friction at the interface. One disadvantage using interface elements is that they have to be predefined in the model. They are hence only suitable for predefined interfaces. For a number of geotechnical problems, e.g., pile installations and retaining walls, the soil-structure interaction can be subjected to large displacements and frictional sliding. Interfaces where sliding and large displacements take place cannot be modelled properly using simplified boundary conditions or traditional interface elements. Using interface elements, sliding along an interface will lead to large distortions of the interface elements. The response can, therefore, be mesh dependent at large displacements.

Contact mechanics

A more rigorous approach, to tackle such problems, is to consider the contact constraint kinematics at the interface. Therefore, computational contact mechanics would be a more fit method to use. However, contact problems that include frictional sliding and large displacements can suffer from numerical instability caused

by the $\mathcal{C}^0$-continuous basis functions used to discretise the geometry in standard finite element method formulations.

3.5 CONCLUSIONS AND MOTIVATION

The interaction between soil and structure can have a large influence on the response of geotechnical structures. As simplified methods are used by engineers in practise, it is important to enlighten how these simplifications affect the design of common structures such as foundations. The first part of this work has, therefore, focussed on evaluating and comparing how simplified methods used in practice affect the design.

For numerical simulation of more complicated structures, the interaction effects between soil and structure can be decisive. For structures where both large relative displacements and sliding take place between the soil and the structure, all methods used today have disadvantages. Recent development using isogeometric analyses (IGA), a numerical method that uses smother shape functions then the conventional finite element method (FEM), has demonstrated improvements to similar applications within other disciplines [19]. Since contact problems are a major part of soil-structure interaction simulations, IGA presents itself as an interesting alternative for analysis of geotechnical problems. Promising results using IGA for fluid flow through porous media have already been presented, [20], [21]. As geotechnical applications often include both complicated contact problems and fluid flow, it is interesting to assess how the isogeometric framework performs for soil plasticity.

4 Geomechanics

Geomechanics is the science in which the mechanical behaviour of soil and rock under loading is studied. Hence, the theoretical frameworks of geomechanics are founded on the pillars of soil and rock mechanics. Even though both soils and rocks are naturally occurring material with some similarities and even though soils are, in general, made up of rock that has been weathered into smaller particles over time, there are important differences between the two materials. In fact at one end rock mechanics grades into soil mechanics, but at the other end, at great depths, rock mechanics grades into the mechanical aspects of structural geology. In turn, the behaviour of a soil can vary greatly depending on the size and shape of the individual particles, the consolidation grade and porosity. Larger particles form frictional soils, such as gravels and sands whereas clayey soils are made up of finer particles. To perform a viable analysis of geotechnical applications it is essential to have a sound understanding of both soil and rock mechanics. This chapter will give a brief introduction of both soil and rock mechanics, which together form the basic theoretical framework for geotechnical analysis.

4.1 SOIL MECHANICS

A soil generally consists of solid particles with intermediate pores filled with air or water. Figure 4.1a illustrates an idealisation of a sand, that has a grain size in the range of 0.063 to 2 mm in diameter. In clayey soil the particles are considerably smaller, with a size less than 2 μm, with flake shape, see Figure 4.1b. The amount of effort that is required to displace a group of particles in a soil influences the compressibility, deformation and strength properties of the soil.

4.1.1 Characteristic behaviour

During analysis of soil behaviour in an engineering practice it is important to have knowledge of both the mechanical and the hydraulic behaviour of the soil. Most

Figure 4.1: Idealisation of a granular and clayey soil where white represent solid particles and grey fluids. a) granular soil. b) clayey soil.

other construction materials, such as concrete, steel and even wood exhibit linear stress-strain behaviour up to well-defined stress limits and the response of these materials can therefore often be analysed using Hooke's law. Soils, however, do not display this linear-elastic behaviour, e.g., a soil in compression becomes gradually stiffer with an increased load. The stiffening behaviour in soil during compression depends on the composition of the material. The reluctance to deform in a soil differs from most other engineering materials, where the deformational resistance is provided from chemical forces binding atoms, molecules and particles together [22]. These forces do exist in soils as well but do not have a great influence on the compression and strength properties. Instead the soil strength properties depend primarily on gravity and on stresses applied to the soil. This has a profound impact on soil behaviour. In a group of particles subjected to pure compression the contact forces between the particles will increase with a decreasing volume, giving the structure of particles a rising strength. Figure 4.2 illustrates the response in a group of particles subjected to pure compression. In Figure 4.2b the compressive stress is given on the vertical axis and the negative volume strain, $\varepsilon_{vol} = \Delta V/V$, on the horizontal axis. The particle structure of soil is also the reason for low or next to non-existing tensile strength of soil, as contact between two particles will not transfer any tensile stresses. If a group of particles, instead, is subjected to a shear force the particles will start to slide over each other, causing large deformations.

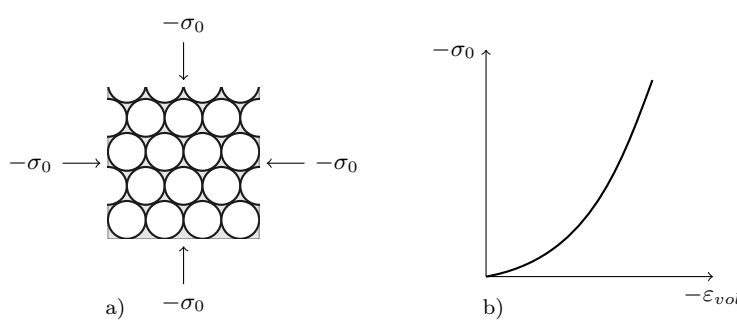

Figure 4.2: a) Soil subjected to compression. b) Generalisation of soil response during compressive loading.

Figure 4.3 illustrates the expected stress-strain behaviour for a group of soil particles subjected to a shear stress. Moreover, by subjecting the group of particles to an isotropic stress the contact forces between the particles get stronger. Hence, the resistance for a shear failure in a soil is increased with an increased isotropic stress.

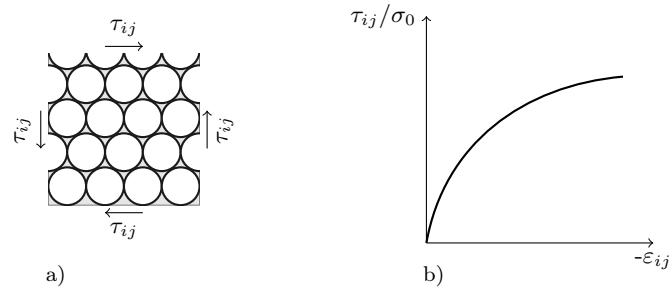

Figure 4.3: a) Soil particles subjected to shear stress. b) Stress-strain relation for a soil during distortion.

Compared to other engineering materials, soil displays rather large deformations at low stress levels. Most of the deformations in soil occur due to particle rearrangement. As the particles cannot be expected to return to their original configuration when unloaded, most soils exhibit irreversible deformations. One can therefore expect to observe permanent deformations in a soil subjected to a loading-unloading cycle. A typical behaviour for a soil subjected to a loading-unloading test is illustrated in Figure 4.4. It can be seen from the figure that during the reloading phase the soil is much stiffer than during the first loading. This behaviour is due to the fact that particles will be less prone to move after the initial loading. The irreversible or plastic strains are denoted as, ε_{ij}^p and the elastic strains are denoted ε_{ij}^e. The total strains are given from

$$\varepsilon_{ij} = \varepsilon_{ij}^e + \varepsilon_{ij}^p \tag{4.1}$$

Effective stress

The structure of soil is of great importance as the particle structure of a soil can carry both normal and shear stress, whereas the liquid and gas phases can carry normal stress but not shear stress [22]. To separate the stress carried by the soil skeleton to the stress carried by the pore water pressure Karl von Terzaghi introduced the concept of effective stress, [23]. Using the concept of effective stress, the total stress σ_{ij} in a soil is defined as

$$\sigma_{ij} = \sigma'_{ij} + u\delta_{ij} \tag{4.2}$$

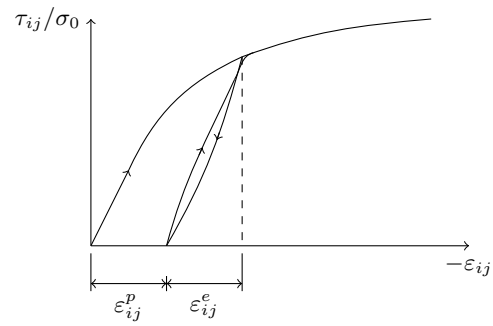

Figure 4.4: Load-reload cycle.

where the effective stress, σ'_{ij}, is the part of the stress carried by the soil particles, and the pore pressure u, is the part of the stress carried by the fluid in the voids. The principle of effective stress contributes to the stress-strain relationship, the change in volume and strength properties of the soil is independent of the pore pressure [22]. As the gas or water filling the pores, generally, is unable to carry shear stress, it is essential to separate the effective stress and the pore water pressure when formulating the stress-strain relations and strength properties of soils. Both the total stress, σ_{ij}, and the pore water pressure, u, can be established from measurements or computed using external and body forces.

Dilatancy

Soils subjected to shear are prone to volume changes. A loose sand will be prone to contract when subjected to shear. Densely packed sand can, however, only deform when particles shear over each other, creating larger space between the particles. The volume increase coupled to shear deformations in soil is called dilatancy and was first discovered by Reynolds in 1885. The dilatancy can have large effect on a soil behaviour as the volume change affects the pore water pressure and in turn the strength of the soil. The dilatancy is often used to govern the potential functions in constitutive modelling of soils [22].

4.1.2 Failure in soil

To model soil behaviour, a number of constitutive models have been developed. These stress-strain relations and strength properties of soils are mathematical equations based on empirical testing. The *Mohr-Coulomb* criterion, was the first constitutive model developed to model soils, and is still one of the most widely used models in soil-mechanics. The criterion states that shear failure τ_f is a function of

the effective normal stress σ' on the shear plane as

$$|\tau_f| = c' - \sigma' \tan \phi' \tag{4.3}$$

where the effective stress σ' is defined as positive in tension. The *cohesion* parameter, c', denotes the intercept for $\sigma' = 0$, and ϕ' is the *internal friction angle*. The Mohr-Coulomb failure criterion will be discussed more thorough later, here it is only presented to illustrate some parameters that are used to describe the shear strength in soils, illustrated in Figure 4.5.

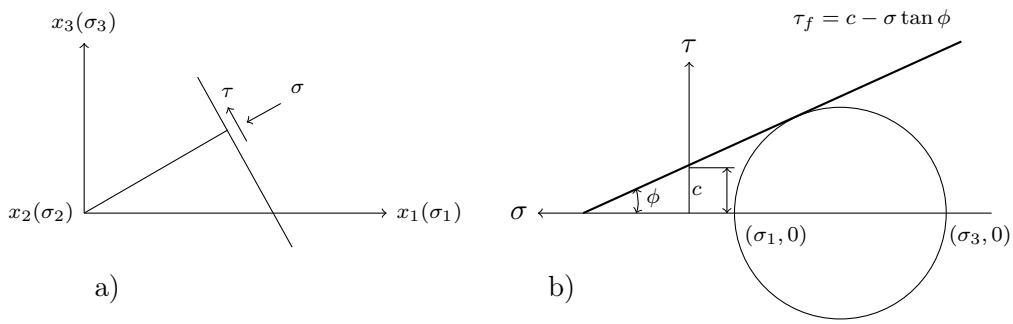

Figure 4.5: a) The failure plane , b) The Coulomb criterion and Mohr's circle.

Moreover, Figure 4.6 illustrates the effect of pore fluid pressure on soil with regard to the Mohr-Coulomb failure criterion, where a) shows the stress state without any existing pore pressure and b) the effective stress. From the figure it becomes clear that an increased pore pressure can lead to failure. It should be noted that the quantity pressure, which conventionally is defined to be positive in compression in this work is chosen to be positive in tension.

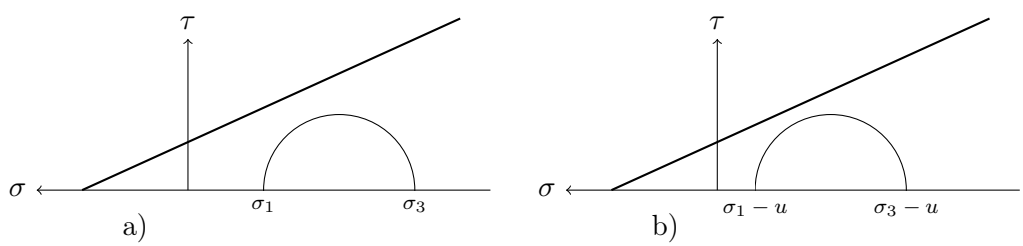

Figure 4.6: The effect on pore pressure of soil, with regard to the Mohr-Coulomb criteria. a) Stress state with no pore fluid pressure. b) Stress state with existing pore fluid pressure.

However, as mentioned earlier the strength of soil in reality may depend on a large number of additional parameters, i.e.,

$$\tau_f = F(c, \phi, \sigma, p, e, C, H, T, \varepsilon, \dot{\varepsilon}) \tag{4.4}$$

where e is the void ratio, C the soil composition, H represents the stress history and T the temperature. The parameter ε denotes, as in the previous, the strain state and $\dot{\varepsilon}$ the strain rate. Depending on the material model used to model the soil behaviour a number of these parameters needs to be established, this is generally done using specific soil tests. Material tests are expensive to preform and simulations of soil behaviour should be conducted in an early stage of any design precess, as the properties of the soil can have a large effect on the overall cost of the project. It is important to have a good understanding of the strength and weaknesses of different constitutive models, so that suitable soil tests can be performed early on in any civil engineering project. Without the right material tests, the results from any analysis can be questionable. To be able to understand and evaluate the credibility of the results from a computational simulation, it is also important to have knowledge of different failure and deformation behaviours for different soils. Some typical stress-strain relations and failure modes for different soils are illustrated in Figure 4.7.

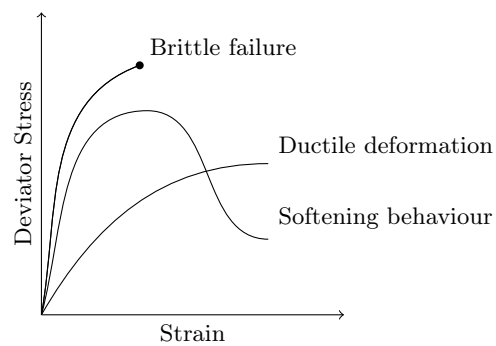

Figure 4.7: Typical stress-strain behaviour for different soils.

The deviator stress on the y-axis in Figure 4.7 is the difference between the major and minor principal stresses in a triaxial test. From Figure 4.7 it can be seen that the stress-strain behaviour ranges from very brittle to ductile behaviour. Table 4.1 indicates the typical failure for soils, useful when evaluating results from analysis [22].

Table 4.1: Typical behaviour for failure of different soils.

quick clays	(Brittle failure)
cemented soils	
heavily overconsolidated clays	
dense sands	
insensitive clays	(Ductile deformation)
remolded clays	
loose sands	

In addition to the parameters mentioned above, there are indeed many other factors that affect how a soil behaves during loading, i.e., load history, effective confining pressure and consolidation rate. The term *consolidation* describes the compaction of a soil, that is, the volume change of a soil as water content is reduced due to an increased overburden or change of the groundwater level.

4.2 ROCK MECHANICS

Most rock consists of a composition of crystals and amorphous particles associated with varying amounts of cementing material. The chemical composition of the crystals may be relatively homogeneous, such as in some limestone, or very heterogeneous, as in granite. The size of the crystals may also vary both in size and distribution, of a typical size no greater than a few centimetres. The crystals generally represent the smallest scale at which the mechanical properties are studied, and deformations of the crystals provide important information about the history of the rock. In addition, the boundary between the crystals represents a weakness in the structure of the rock, which otherwise can be seen as continuous. However, rock mechanics is mostly focussed on rock masses ranging from a few metres up to hundreds of metres, the scale commonly found within civil engineering projects and the mining industry. On this scale there are often existing cracks, joints and faults that form discontinuities in a rock mass. These structural features will have an effect on the overall mechanical properties of the rock mass. The ability to numerically model the behaviour of rock masses is essential to many problems that geotechnical engineers encounter and to realistically reproduce rock mass behaviour it is necessary to determine the numerical values of the rock's mechanical properties, i.e., Young's modulus, density and Poisson's ratio. For practical purposes the material properties are best obtained from laboratory measurements made on smaller rock specimens. These specimens are, in general, too small to capture the overall properties of a large rock mass, but of a sufficient size to contain enough structural

variations to adequately give a homogeneous representation of the intact rock.

4.2.1 Characteristic behaviour

The fact that rocks are a composition of compressed particles often makes them heterogeneous and porous in nature, which in turn results in a complex behaviour during external loading. To get a better understanding of the characteristic behaviour of intact rock during external loading we consider rock specimen subjected to uniaxial compression. Figure 4.8 displays a typical stress-strain curve from a uniaxial compression test of a rock specimen. From the stress-strain curve it is possible to identify three distinct segments during the loading before the peak stress, or uniaxial compressive strength, σ_c is reached. Generally the first part of the stress-strain curve for rock under uniaxial compression can be identified by a positive second derivative, which may occur due to closing of voids or flaws in the specimen. The second part of the curve is often close to linear, and moreover, during the first two segments the stress-strain behaviour is generally nearly elastic. However, at around 50-70 % of the compressive strength, σ_c, irreversible micro cracks start to appear and a softening behaviour can be observed in the stress-strain curve, i.e., part three in Figure 4.8.

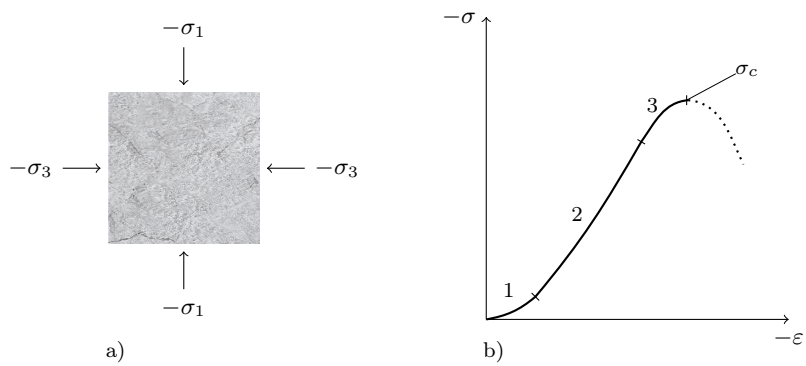

Figure 4.8: a) Rock specimen subjected to compression. b) Characteristic stress-strain behaviour for a rock specimen during compression.

It is important to realise that the peak stress σ_c, the uniaxial compressive strength, is not an intrinsic material property, i.e., it depends on both the loading conditions and the geometry of the specimen. An increased ratio between width and height of the rock specimen will lead to an increase in compressive strength as well as a more ductile failure process. A similar effect can be seen if a rock specimen is subjected to a confining pressure during a compression test, see Figure 4.9.

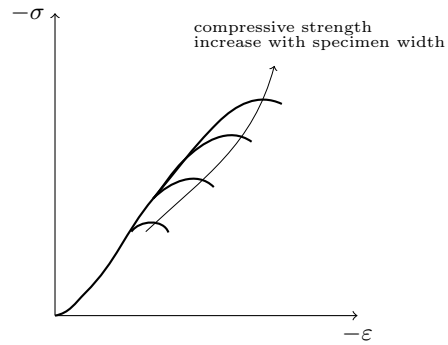

Figure 4.9: Representation of how the width/height ratio of the rock specimen affects the compressive strength during uniaxial compression tests.

Another important aspect of rock behaviour is that rocks in general are porous to some extent, and the pores are typically filled with fluids or gas under pressure. The pore fluid can influence failure of a rock in mainly two ways; either by mechanical effects from the pore pressure, or due to chemical interaction between the rock and the fluid. Work on the effects of chemical interaction between rock and pore fluid can be found in, i.e., [15]. The mechanical effect of pore pressure acting outward from the pore space and therefore acting like tensile stress on the rock and may lead to a reduced compressive strength of the rock specimen. This behaviour is supported experimentally for most rocks, that is to say, the principle of effective stress presented in equation (4.2) also hold for rocks.

Failure in rock

In rock mechanics, failure generally refers to when a rock suffers irreversible damage, permanently affecting its load-bearing ability. A number of constitutive models have been introduced to predict the failure conditions of rocks, i.e., Mohr-Coulomb and Hoek and Brown. Although existing failure criteria are widely used and capable of predicting the overall strength values and behaviour of rock during external loading, these criteria may not be able to satisfactorily describe the failure process in detail. As for most rock, failure is essentially a process of crack initiation and propagation, the use of fracture mechanics has therefore become a common tool to study the detailed failure process in rock. As mentioned previously, the loading condition and geometry of a rock specimen will influence both the strength and failure process of a rock subjected to external loads. A rock specimen subjected to unconfined compression will typically display an elastic behaviour until abrupt failure takes place. The failure process in rock during unconfined compression does generally take place through the formation of brittle fractures in the loading direction, illustrated in Figure 4.10a.

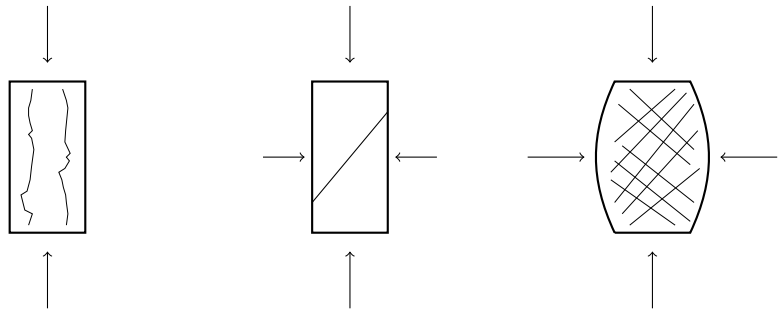

Figure 4.10: Representation of characteristic fracture processes for rock specimens subjected to external loading. a) Rock specimen subjected to uniaxial compression b) Shear fracture in a rock specimen with a moderate confining pressure. c) Network of shear fractures during ductile failure in a rock specimen with an increased confining pressure.

If the confining pressure is increased during compression, the failure process will change. For moderate confining pressures, failure will take place through the formation of shear fractures, see Figure 4.10b). With further increased confining pressure the failure process will change from brittle to ductile, where a network of shear fractures will be formed in the specimen, see Figure 4.10c).

4.2.2 Griffith theory for brittle fractures

Modern fracture mechanics stem from Griffith's theory for brittle fractures, which states that propagation of fractures is the source for failure of loaded brittle materials, and provides a description for formation of discontinuities in an unbroken structure. Griffith's work was first presented in 1921, and was motivated by the contradiction that the theoretical stress value needed to break the atomic bond in glass was approximately 100 times greater than the stress needed to fracture bulk glass. Griffith stipulated that the difference in theoretical and experimental values was due to the presence of sub-microscopic flaws or micro-cracks in the material. Griffith showed that the product of the square root of the length of the flaw and the stress at fracture was close to constant. However, this relation poses a mathematical difficulty, for a perfectly sharp crack the stresses approach infinity at the crack tip. To overcome this problem, Griffith developed a thermodynamic approach and found that for a perfect elastic material failure occurs when the surface energy reaches a peak value at a critical crack length, after which the surface energy decrees as the

crack length increases, i.e.

$$\sigma_f \sqrt{a} = \sqrt{\frac{2E\gamma}{\pi}} \tag{4.5}$$

where σ_f is the applied stress at failure, a half the length of the crack, E the Young's modulus and γ the surface energy. Griffith's work led to the introduction of the term strain energy release rate, $\mathcal{G}$, which describes the rate at which the energy is absorbed during crack growth. In other terms, a crack will grow when the energy released by the body per unit fracture area is greater than or equal to the increase in surface energy

$$\mathcal{G} \geq 2\gamma \tag{4.6}$$

Moreover, Irwin, [24], and Orowan, [25], independently discovered that, for more ductile materials, the released strain energy could not be absorbed by the formation of new fracture surfaces. Instead, they suggested that the released strain energy to a large extent was dissipated due to plastic flow in a zone near the crack tip, which in rock may consist of crushed grains and micro-cracking. To accommodate for this plastic zone, they suggested that catastrophic fractures occur when the strain energy release rate reaches a critical value, $\mathcal{G}_c$. For brittle materials, the critical strain energy release rate, $\mathcal{G}_c$, is generally considered a material parameter even though in practice it depends on loading conditions and the geometry of the crack. Measured values of the critical energy release rate $\mathcal{G}_c$ for various rocks and minerals have been compiled by [26]. By choosing a sufficiently small crack size and with known value of $\mathcal{G}_c$ for a given material, it is possible to establish a safe level of stress, σ_f. For a simple case of a thin plate with a crack perpendicular to the load, see Figure 4.11 and assuming plane stress, it is possible to determine the peak stress from

$$\sigma_f = \sqrt{\frac{E\mathcal{G}_c}{\pi a}} \tag{4.7}$$

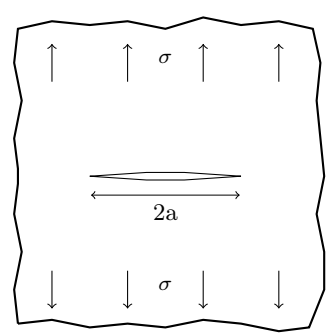

Figure 4.11: A thin rectangular plate with a crack of length 2a perpendicular to the load.

Note that the Griffith theory can be further generalized to consider any cracked body, by using an energy balance between the decrease in potential energy Π at an

infinitely small increase in crack area A, i.e

$$\mathcal{G} = -\frac{\partial \Pi}{\partial A} = -\frac{\partial}{\partial A}(U_e + U_p) \tag{4.8}$$

where U_p and U_e are the potential and elastic energy of the load respectively. Moreover, fractures can be decomposed into three different fracture modes. Where Mode I represents fractures in pure tension, Mode II represents in-plane shear fractures and Mode III anti-plane shear fractures, see Figure 4.12. Similarly, the strain energy release rate can be decomposed into three modes, as $mathcalG = mathcalG_I + mathcalG_{II} + mathcalG_{III}$.

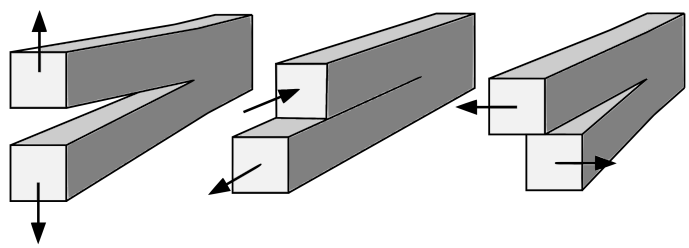

a) b) c)

Figure 4.12: a) The different fracture modes. a) Mode I fracture. b) Mode II fracture. c) Mode III fracture.

4.3 FAILURE CRITERIA

Numerical simulations can be of great use when analysing the behaviour of geomaterials for complex construction projects, and a number of sophisticated constitutive models have been developed in the science community. However, engineers working with analysis of geomaterials, often prefer less complex constitutive models when preforming analysis. So, even though there exists a number of sophisticated constitutive models to model both soil and rock behaviour, it is important to understand the pros and cons of the models widely used by practising engineers. This section will present two of the most basic criteria used to model failure in soils and rock, namely the Mohr-Coulomb criterion and Drucker-Prager criterion.

4.3.1 Mohr-Coulomb criterion

The failure criterion often referred to as the Mohr-Coulomb failure criterion is the most popular failure criterion in soil mechanics and was first presented in 1773

by Charles-Augustin de Coulomb, and was the first criterion to account for the hydrostatic stress. According to the Mohr-Coulomb criterion the shear strength increases with increasing compressive stress,

$$|\tau_f| = c' - \sigma' \tan \phi' \tag{4.9}$$

where τ_f is the shear stress on the failure plane, c' the material cohesion, σ' the normal effective stress on the failure surface and ϕ' the angle of internal friction. In Figure 4.13 the Mohr-Coulomb criterion is illustrated employing the Mohr circle. With Figure 4.13 as reference the Mohr-Coulomb criterion is derived as

$$\frac{\sigma_1' - \sigma_3'}{2} = AB + BF \tag{4.10}$$

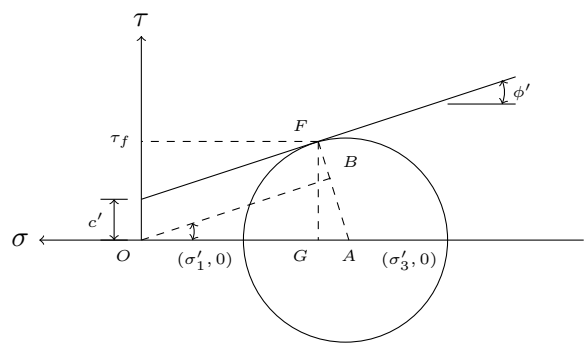

Figure 4.13: The Mohr-Coulomb criterion and Mohr's circle.

which can be rewritten as,

$$\frac{\sigma_1' - \sigma_3'}{2} = OA \sin \phi' + c' \cos \phi' \tag{4.11}$$

Inserting that $OA = -\frac{1}{2}(\sigma_1' + \sigma_3')$ into (4.11) one obtains,

$$-\frac{\sigma_1' - \sigma_3'}{2} = \frac{\sigma_1' + \sigma_3'}{2} \sin \phi' - c' \cos \phi' \tag{4.12}$$

where σ_1' and σ_3' are the major and minor principal effective stress respectively. It is also clear from (4.12) that the Mohr-Coulomb criterion is independent of the effects of the intermediate principal effective stress, σ_2' [27]. The expression in (4.12) can be projected on the deviator- or π-plane where it takes the form of an irregular hexagon illustrated in Figure 4.14.

The Mohr-Coulomb criterion states that the yield strength in compression is higher than the yield strength in tension. The Mohr-Coulomb criterion is expressed in

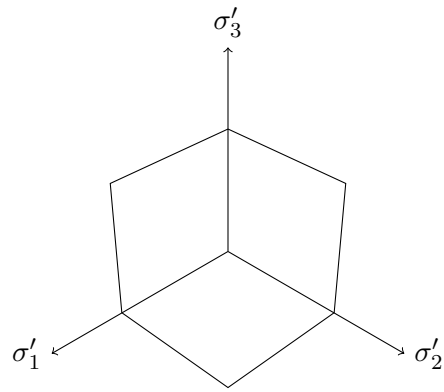

Figure 4.14: The Mohr-Coulomb criterion on the deviator plane.

terms of σ_1' and σ_3', and is, as mentioned, not including σ_2'. It is therefore inconvenient to express the Mohr-Coulomb criterion with the components of the stress tensor and consequently it becomes difficult to describe the criterion with the stress invariants (I_1, I_2, I_3). The Mohr-Coulomb yield criterion is instead commonly described using the first invariant of the stress tensor I_1, the second invariant of the deviatoric stress tensor J_2 and the Lode angle θ. The representation of the invariants is described using the full stress tensor, σ_{ij}. For geo-materials the stress tensor is often substituted with the effective stress tensor, σ_{ij}'. For the special case where no pore water pressure is present $\sigma_{ij} = \sigma_{ij}'$. The *deviator stress tensor* is defined as

$$s_{ij} = \sigma_{ij} - \frac{1}{3}\sigma_{kk}\delta_{ij} \tag{4.13}$$

and the first stress invariant is given from

$$I_1 = \sigma_{ii} \tag{4.14}$$

The second invariant of the deviator stress tensor is calculated as

$$J_2 = \frac{1}{2}s_{ij}s_{ji} \tag{4.15}$$

Finally the Lode angle, θ is defined as

$$\theta = -\tfrac{1}{3}\sin^{-1}\Big(-\frac{3\sqrt{3}}{2}\frac{J_3}{J_2^{3/2}}\Big) \tag{4.16}$$

where $-\pi/6 \leq \theta \leq \pi/6$ and $J_3 = \frac{1}{3}(s_{ij}s_{jk}s_{ki})$. This leads to the convectional form of Mohr-Coulomb criterion in a three-dimensional stress space as, [27]

$$f(I_1, J_2, \theta) = I_1 \sin\phi' + \sqrt{J_2}\cos\theta - \frac{\sqrt{J_2}}{3}\sin\phi'\sin\theta - c'\cos\phi' = 0 \tag{4.17}$$

One setback to the Mohr-Coulomb criterion is that the shape of the yield surface leads to numerical difficulties when treating the plastic flow at corners of the yield surface. Another issue with the Mohr-Coulomb criterion is the conic shape of the yield surface opening in the direction of the hydrostatic axis, see Figure 4.15. This leads to that the Mohr-Coulomb criterion will not describe soil behaviour accurately above a certain limit pressure. The opening in the direction of the hydrostatic axis implies that the material can bear infinite pure hydrostatic compressions without forming any plastic deformations [28].

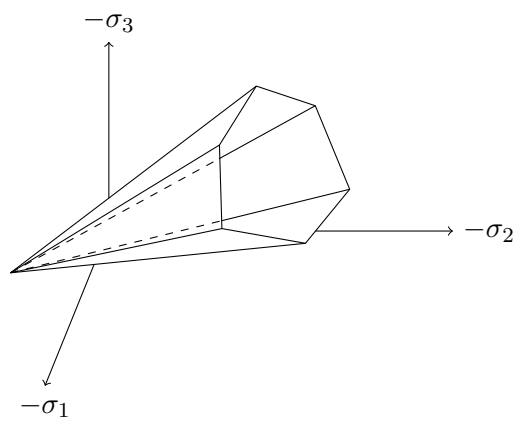

Figure 4.15: Projection of the Mohr-Coulomb criterion in the principal stress space.

4.3.2 Drucker-Prager criterion

The Drucker-Prager criterion was suggested by Drucker and Prager in 1952 and it can be seen a generalisation of the Mohr-Coulomb criterion to account for the effects of all principal stresses. This generalisation is formed using the first invariant of the stress tensor, I_1, and the second invariant of the deviatoric stress tensor, J_2 as

$$f(I_1, J_2) = \sqrt{J_2} - \alpha I_1 - k = 0 \tag{4.18}$$

The parameters α and k are positive material parameters that can be determined from the slope and interception of the yield surface plotted in the $I_1 - \sqrt{J_2}$ plane, illustrated in Figure 4.16. The values of k and α can also be expressed in terms of cohesion, c', and internal friction, ϕ'. For the conventional triaxial tests, i.e., where $\sigma_2 = \sigma_3$, the parameters k and α can be determined either by matching to the compressive meridian of the Mohr-Coulomb criterion by

$$\alpha = \frac{2}{\sqrt{3}} \frac{\sin \phi'}{(3 - \sin \phi')} \tag{4.19}$$

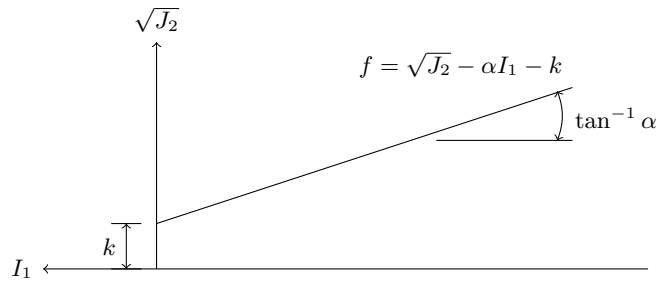

Figure 4.16: The Ducker-Prager criterion in the meridian plane.

$$k = \frac{6}{\sqrt{3}} \frac{c' \cos\phi'}{(3 - \sin\phi')} \tag{4.20}$$

or matching the tensile meridian of the Mohr-Coulomb criterion using

$$\alpha = \frac{2}{\sqrt{3}} \frac{\sin\phi'}{(3 + \sin\phi')} \tag{4.21}$$

$$k = \frac{6}{\sqrt{3}} \frac{c' \cos\phi'}{(3 + \sin\phi')} \tag{4.22}$$

The matching of the Drucker-Prager criterion to either the compressive or the tensile meridian of the Mohr-Coulomb criterion is illustrated in Figure 4.17. From Figure

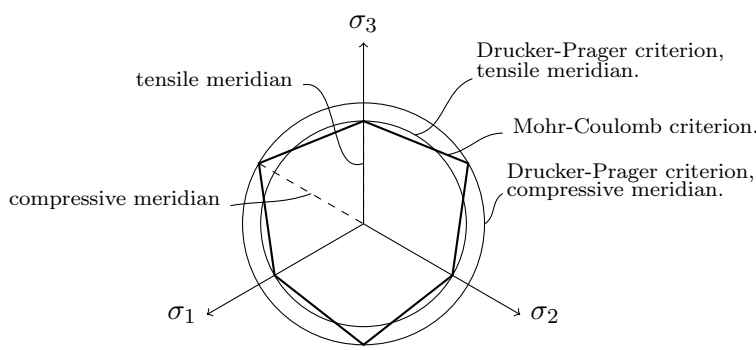

Figure 4.17: Projection of the Drucker-Prager criterion matched to the Mohr-Coulomb criterion on the deviator plane.

4.17 it can be seen that the Drucker-Prager criterion takes the form of a circle when viewed in the deviator plane. This property of the Drucker-Prager criterion makes it more stable in numerical calculations than the Mohr-Coulomb criterion. One drawback that the Ducker-Prager criterion has in common with the Mohr-Coulomb criterion is the conic shape of the yield surface that is open in the direction of the hydrostatic axis, see Figure 4.18 [27]. This leads to that the models allow

for unlimited hydrostatic stresses without any plastic deformations taking place. However, it is possible to remedy this limitation by adding a second yield surface often referred to as a cap, to the model. Lastly, it is well worth noting that, even

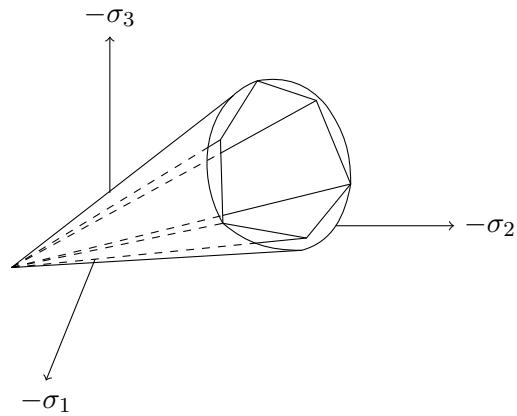

Figure 4.18: The Drucker-Prager criterion matched to the compressive meridian of the Mohr-Coulomb criterion in the principal stress space.

though the Drucker-Prager criterion is an approximation of the Mohr-Coulomb criterion that presents some benefits regarding numerical stability, it is in general not regarded to be a good fit for simulation of soil-behaviour. The disadvantages are well known in the science community and it is only for very homogeneous stress states that the model gives acceptable results.

5 Numerical modelling of geomaterials

This chapter will give an overview of the theories and numerical methods used to simulate soil and rock behaviour in this work. The chapter starts with a brief description of linear and non-linear elasticity followed by a presentation of the theory of plasticity used to simulate soil behaviour in Paper B. The chapter continues with an outline of the phase-field fracture model used to simulate brittle fractures in rock presented in Paper C and Paper D. The chapter is concluded with a description of the numerical methods used to conduct the simulations in this work. A more detailed description on the numerical methods can be found in the appended papers presented in Part II of this work.

5.1 MODELLING OF SOIL BEHAVIOUR

This section will present the basic theories needed to model the complex behaviour of soil under loading. As soils differ to other construction materials, such as concrete or steel which exhibit linear stress-strain behaviour up to a well-defined stress limit, it is often necessary to model the behaviour of soil using non-linear elasticity or plasticity. We will start this section by giving a definition of the concept of strain. The section will continue with a brief outline of linear elasticity, as, even though it is of limited use for modelling of soil response, it is a natural starting point of constitutive modelling. As mentioned in Chapter 4 a number of constitutive models have been developed to model soil behaviour. Even though the models vary in complexity, most models developed for simulation of soil behaviour rely on the theory of plasticity. Therefore the section will be concluded with a general introduction to plasticity.

5.1.1 Strain

Consider a point A in an undeformed body that can be described by the coordinates (x_1, x_2, x_3) see Figure 5.1. If the body is deformed, the point A will be moved to A* and described by the coordinates (x_1^*, x_2^*, x_3^*), where

$$x_i^* = x_i + u_i \tag{5.1}$$

u_1, u_2 and u_3 describe the displacements in the x_1, x_2 and x_3 directions over time. The displacements are often written as

$$u_i = u_i(x_i, t) \tag{5.2}$$

Now consider an adjacent point B in the body as shown in Figure 5.1. Let the point be described by the coordinates $(x_i + dx_i)$, where dx_i denotes the distance in the x_i direction between point A and B prior to deformation. Point B will in conformity with point A be moved to B* after a deformation of the body. The point B* will be described by the coordinates $(x_1^* + dx_1^*, x_2^* + dx_2^*, x_3^* + dx_3^*)$, where

$$x_i^* + dx_i^* = x_i + dx_i + u_i + du_i$$

in which,

$$du_i = u_{i,j} dx_j \tag{5.3}$$

where $u_{i,j}$ is the *displacement gradient*, defined as

$$u_{i,j} = \frac{\partial u_i}{\partial x_j} \tag{5.4}$$

The distance from point A to point B prior to deformation, is given by dx_i, see Figure 5.1. In the following the length of the vector from A to B will be denoted $|\overrightarrow{AB}|$.

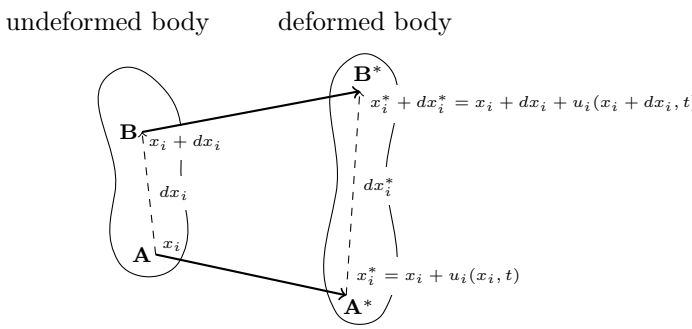

Figure 5.1: Illustration of displacements of neighboring material points.

Due to the deformation of the body, the distance dx_i is changed according to Figure 5.1. The distance in the x_i direction between A* and B* in the deformed configuration is obtained from $(x_i^* + dx_i^*) - x_i^*$ which, using equation (5.1)-(5.3), can be written as:

$$dx_i^* = dx_i + du_i = (\delta_{ij} + u_{i,j})dx_j \tag{5.5}$$

where δ_{ij} is the Kronecker delta. Using the same notation as in the undeformed configuration, the length of the vector from A* to B* is denoted $|\overrightarrow{A^*B^*}|$, giving that

$$|\overrightarrow{A^*B^*}|^2 = (\delta_{ki} + u_{k,i})(\delta_{kj} + u_{k,j})dx_i dx_j \tag{5.6}$$

Using that $|\overrightarrow{AB}|^2 = dx_j dx_j$ and that $dx_j dx_j = dx_i dx_j \delta_{ij}$ together with equation (5.6) the difference between $|\overrightarrow{A^*B^*}|^2$ and $|\overrightarrow{AB}|^2$ can be written as

$$|\overrightarrow{A^*B^*}|^2 - |\overrightarrow{AB}|^2 = (u_{i,j} + u_{j,i} + u_{k,i}u_{k,j})dx_i dx_j \tag{5.7}$$

This equation may be rewritten as

$$|\overrightarrow{A^*B^*}|^2 - |\overrightarrow{AB}|^2 = 2dx_i E_{ij} dx_j \tag{5.8}$$

where the *Green strain tensor*, E_{ij} is given by

$$E_{ij} = \tfrac{1}{2}(u_{i,j} + u_{j,i} + u_{k,i}u_{k,j}) \tag{5.9}$$

The Green strain tensor is a second-order symmetric tensor and it was first introduced by Green in 1841. For the work presented in this dissertation, small strains are assumed. Hence, the *small displacement gradient* will be considered, consequently the quadratic term of equation (5.9) is ignored. This simplification can be expressed by replacing E_{ij} in equation (5.8) with the *small strain tensor*, ε_{ij} given by

$$\varepsilon_{ij} = \tfrac{1}{2}(u_{i,j} + u_{j,i}) \tag{5.10}$$

5.1.2 Linear elasticity

Experimental observations have shown that many materials behave linear elastically up to a certain stress level. For isotropic materials exhibiting linear elastic behaviour the relation between stresses and strains can be defined by two material properties, namely *Young's modulus*, also referred to as *elasticity modulus*, and *Poisson's ratio*, denoted E and ν respectively.

With the help of these properties, a relation between the stress and strain tensor can be formed as a fourth-order elasticity tensor D_{ijkl} called the *stiffness tensor*. Though it would be possible to form the stiffness tensor using Young's modulus

and Poisson's ratio, it can be useful to express the stress-strain relation using the *shear modulus*, μ, and the *bulk modulus*, K given by

$$\mu = \frac{E}{2(1+\nu)} \tag{5.11}$$

$$K = \frac{E}{3(1-2\nu)} \tag{5.12}$$

Using these quantities a stress-strain relation can be formulated as

$$\sigma_{ij} = 3K\Big(\frac{1}{3}\varepsilon_{kk}\delta_{ij}\Big) + 2\mu\Big(\varepsilon_{ij} - \frac{1}{3}\varepsilon_{kk}\delta_{ij}\Big) \tag{5.13}$$

or in a much useful manner using that $\varepsilon_{ij} = \frac{1}{2}(\delta_{ik}\delta_{jl} + \delta_{il}\delta_{jk})\varepsilon_{kl}$

$$\sigma_{ij} = 2\mu\Big[\frac{1}{2}(\delta_{ik}\delta_{jl} + \delta_{il}\delta_{jk}) + \frac{\nu}{1-2\nu}\delta_{ij}\delta_{kl}\Big]\varepsilon_{kl} \tag{5.14}$$

From this expression it is evident that the first part on the right-hand side can be recognised as the stiffness tensor, that is

$$D_{ijkl} = 2\mu\Big[\frac{1}{2}(\delta_{ik}\delta_{jl} + \delta_{il}\delta_{jk}) + \frac{\nu}{1-2\nu}\delta_{ij}\delta_{kl}\Big] \tag{5.15}$$

Using D_{ijkl}, the constitutive relation between stresses and strains for an isotropic linear elastic material can then be written as

$$\sigma_{ij} = D_{ijkl}\varepsilon_{kl}, \tag{5.16}$$

which is recognized as *Hooke's generalised law* for isotropic elasticity and was in a uniaxial form suggested by Robert Hooke in 1676. As D_{ijkl} is an isotropic fourth-order tensor and σ_{ij} and ε_{ij} are second order tensors, it is possible to invert equation (5.16) to determine the strains as

$$\varepsilon_{ij} = C_{ijkl}\sigma_{kl}, \tag{5.17}$$

where C_{ijkl} is called the *elastic isotropic flexibility tensor* [28], given by.

$$C_{ijkl} = \frac{1}{2\mu}\Big[\frac{1}{2}(\delta_{ik}\delta_{jl} + \delta_{il}\delta_{jk}) - \frac{\nu}{1+\nu}\delta_{ij}\delta_{kl}\Big]. \tag{5.18}$$

5.1.3 Theory of plasticity

Linear elasticity is in most cases too crude to model the essential features of soil behaviour, as they show irreversible, or plastic, deformations at relatively small stresses. In general, if the stress state exceeds the yield strength of the material, plastic strains, ε^p_{ij}, will develop. For soils the yield strength is dependent on the

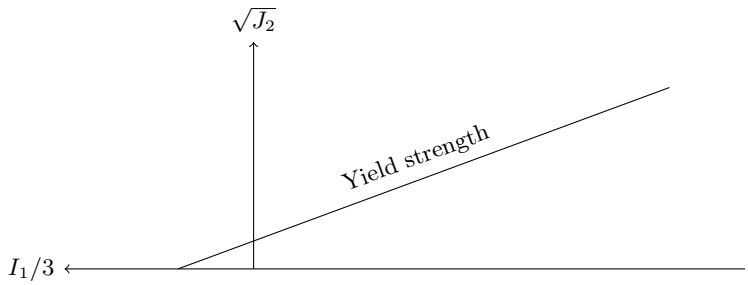

Figure 5.2: Yield strength of a friction material viewed in the meridian plane.

hydrostatic pressure, as illustrated in Figure 5.2. One characteristic behaviour of materials that suffer irreversible deformations, ε_{ij}^p, is that the reloading path differs from the original loading path, see Figure 5.3. This implies that the material behaviour is no longer only determined from current stress state but rather said to be history dependent, i.e., it can only be determined by an integration of the load history [28]. This is illustrated in Figure 5.3, where it is obvious that the strains are equal at different stress levels along the dotted line.

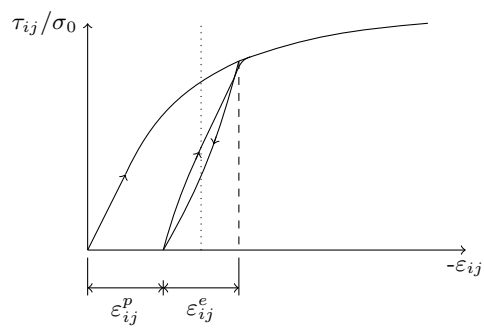

Figure 5.3: Load-reload cycle.

To capture the behaviour illustrated in Figure 5.3, the total strain ε_{ij} is divided into two parts, where the irreversible or plastic strains are denoted as, ε_{ij}^p and ε_{ij}^e represents the elastic strains,

$$\varepsilon_{ij} = \varepsilon_{ij}^e + \varepsilon_{ij}^p. \tag{5.19}$$

Due to the dependence on the load history, constitutive models for plasticity are written in an incremental from, with their corresponding incremental plastic strains or *plastic strain rates*, denoted $\dot{\varepsilon}_{ij}^p$. However, $\dot{\varepsilon}_{ij}^p$, is used instead of $d\varepsilon_{ij}^p$ plainly to simplify the notation. For elastic-ideal plastic materials the plastic part of $\dot{\varepsilon}_{ij}$ can be determined from

$$\dot{\varepsilon}_{ij}^p = \dot{\beta} s_{ij} \qquad \dot{\beta} \geq 0 \tag{5.20}$$

where s_{ij} represents the deviatoric stress tensor. The constitutive relation for $\dot{\varepsilon}^p_{ij}$ is called the *flow rule*. The original flow rule assumes that the material is incompressible under plastic flow or yielding, i.e., that the volumetric strain tensor $\varepsilon^p_{ii}/3$ is equal to zero. This is, however, generally not true for geological materials [27]. As this work deals with friction materials, a constitutive expression suitable for geomaterials will be used to illustrate the flow rule. For this case the Drucker-Prager yield criterion has been used as it is relatively simple compared to other constitutive models. According to equation (4.17),

$$f(\sigma_{ij}) = \sqrt{J_2} - \alpha I_1 - k \tag{5.21}$$

where k and α are presented in equation (4.19)-(4.20). Differentiating equation (5.21), it becomes

$$\frac{\partial f}{\partial \sigma_{ij}} = -\alpha \delta_{ij} + \frac{s_{ij}}{2\sqrt{J_2}} \tag{5.22}$$

Combining equation (5.22) with equation (5.20), an expression to determine the direction of the plastic strains can be obtained:

$$\dot{\varepsilon}^p_{ij} = \dot{\lambda} \frac{\partial f}{\partial \sigma_{ij}} \qquad \dot{\lambda} \geq 0 \tag{5.23}$$

where $\dot{\lambda}$ is called the so called *plastic multiplier*, which regulates the magnitude of the plastic strains. For the Drucker-Prager criterion the plastic multiplier can be determined from

$$\dot{\lambda} = \Big(\frac{s_{ij}}{\alpha \delta_{ij}} + 2\sqrt{J_2} \Big) \dot{\beta}. \tag{5.24}$$

Until the stress state reaches the yield surface, that is, while $f < 0$, the quantity $\frac{\partial f}{\partial \sigma_{ij}}$ can be seen as the normal to the yield surface $f = 0$, illustrated in Figure 5.4.

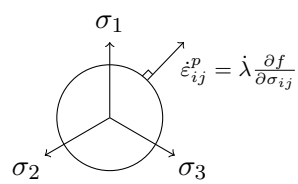

Figure 5.4: Normality of the incremental plastic strains.

As the normal to the yield surface is given from equation (5.24), the yield surface f can be seen as a potential function for the incremental plastic strains. Using more general terms the flow rule can be written as

$$\dot{\varepsilon}^p_{ij} = \dot{\lambda} \frac{\partial g}{\partial \sigma_{ij}} \qquad \dot{\lambda} \geq 0 \tag{5.25}$$

where g represents a non-specific *potential function*, that can take other forms than the yield surface f. The potential function, g, is in general determined with the same quantities as the yield surface.

$$g(\sigma_{ij}) = 0 \tag{5.26}$$

If $g = f$ the flow rule is said to be *associated*. The use of *associated flow rule* has shown good numerical results compared to material testing of metals and non-friction materials. However, for friction materials, experimental and numerical results have proven to diverge when the associated flow rule has been used, [28]. Therefore, a potential function, not equal to the yield surface, i.e., $g \neq f$, is used in most constitutive models for geo-materials. The total incremental strain can be expressed using its elastic and plastic parts,

$$\dot{\varepsilon}_{kl} = \dot{\varepsilon}^e_{kl} + \dot{\varepsilon}^p_{kl} \tag{5.27}$$

Inserting the incremental equation (5.27) into equation (5.16) we get,

$$\dot{\sigma}_{ij} = D_{ijkl}(\dot{\varepsilon}_{kl} - \dot{\varepsilon}^p_{kl}). \tag{5.28}$$

Inserting the flow rule from equation (5.25) the expression changes into

$$\dot{\sigma}_{ij} = D_{ijkl}\dot{\varepsilon}_{kl} - \dot{\lambda} D_{ijst}\frac{\partial g}{\partial \sigma_{st}}. \tag{5.29}$$

To solve for the magnitude of the plastic strains, $\dot{\lambda}$, we utilise that the gradient $\partial \mathrm{g}/\partial\sigma_{ij}$ describes the direction of the plastic strains. As the stress state per definition will be located on the yield surface, the plastic loading will always be located on the yield surface [28], that is $f(\sigma_{ij} = 0)$. The variation of the stress state so that it remains on the yield surface during plastic loading is governed by the so-called *consistency relation*

$$\frac{\partial f}{\partial \sigma_{ij}}\dot{\sigma}_{ij} + \frac{\partial f}{\partial K_\alpha}\dot{K}_\alpha = 0 \tag{5.30}$$

where, K_α describes a hardening parameter which in turn is dependent on the internal variable κ_α. It is important to acknowledge that the relation between K_α and κ_α is established for the specific material properties of interest. However, it is possible to express this in a more general manner by introducing the *evolution functions* k_α. This is done by first inserting the internal variable into equation (5.30), obtaining,

$$\frac{\partial f}{\partial \sigma_{ij}}\dot{\sigma}_{ij} + \frac{\partial f}{\partial K_\alpha}\frac{\partial K_\alpha}{\partial \kappa_\beta}\dot{\kappa}_\beta = 0. \tag{5.31}$$

Introducing k_α as variables describing how κ_α evolves with the plastic deformation, the *evolution laws* can be established accordingly,

$$\dot{\kappa}_\alpha = \dot{\lambda} k_\alpha(\sigma_{ij}, K_\beta) \tag{5.32}$$

That $\dot{\lambda}$ is a part of the internal variable is not unexpected as it was earlier mentioned that $\dot{\lambda}$ controls the magnitude of $\dot{\varepsilon}^p_{ij}$. Inserted in the consistency relation, equation (5.30) we obtain,

$$\frac{\partial f}{\partial \sigma_{ij}}\dot{\sigma}_{ij} + \dot{\lambda}\frac{\partial f}{\partial K_\alpha}\frac{\partial K_\alpha}{\partial \kappa_\beta}k_\beta = 0 \tag{5.33}$$

Multiplying equation (5.29) with $\partial f/\partial \sigma_{ij}$ and using equation (5.33) and (5.25) it is possible to form an expression to determine $\dot{\lambda}$, as

$$\dot{\lambda} = \frac{1}{A}\frac{\partial f}{\partial \sigma_{ij}}D_{ijkl}\dot{\varepsilon}_{kl}; \qquad \dot{\lambda} \geq 0 \tag{5.34}$$

where A is defined by

$$A = H + \frac{\partial f}{\partial \sigma_{ij}}D_{ijkl}\frac{\partial g}{\partial \sigma_{kl}} \qquad A > 0 \tag{5.35}$$

H, represents the plastic modulus, which governs hardening behaviour. For non-hardening plasticity $H = 0$. Inserting the expression for $\dot{\lambda}$ into the flow rule equation (5.25), it turns out that the plastic part of the strain tensor can be established when the total strains are known

$$\dot{\varepsilon}^p_{ij} = \frac{1}{A}\Big(\frac{\partial f}{\partial \sigma_{kl}}D_{klmn}\dot{\varepsilon}_{mn}\Big)\frac{\partial g}{\partial \sigma_{ij}} \tag{5.36}$$

This implies that, if the total strain rates are known, the total stress rates can be determined from

$$\dot{\sigma}_{ij} = D^{ep}_{ijkl}\dot{\varepsilon}_{kl} \tag{5.37}$$

The *elasto-plastic stiffness tensor*, D^{ep}_{ijkl}, which determines the current *tangential stiffness* of the material is defined as

$$D^{ep}_{ijkl} = D_{ijkl} - \frac{1}{A}D_{ijst}\frac{\partial g}{\partial \sigma_{st}}\frac{\partial f}{\partial \sigma_{mn}}D_{mnkl} \tag{5.38}$$

The expression in equation (5.37) is the sought general form of the stress-strain relation. It was first established by Hill in 1958 for associated plasticity and later in 1966 by Mroz for general non-associated plasticity [28]. There are a few properties of the elasto-plastic stiffness tensor worth emphasising. Foremost, it can be observed that D^{ep}_{ijkl} does not depend on neither $\dot{\sigma}_{ij}$ nor $\dot{\varepsilon}_{ij}$ which results in that equation (5.37) is incrementally linear. Furthermore D^{ep}_{ijkl} shows similar symmetric properties as the stiffness tensor from equation (5.15), that is

$$D^{ep}_{ijkl} = D^{ep}_{jikl} \qquad D^{ep}_{ijkl} = D^{ep}_{ijlk}$$

For associated plasticity it also yields that $D^{ep}_{ijkl} = D^{ep}_{klij}$, which does not hold for non-associated plasticity, i.e. $D^{ep}_{ijkl} \neq D^{ep}_{klij}$. For numerical calculations using non-linear FEM or IGA it is of importance that equation (5.37) can be written on matrix form [28],

$$\dot{\boldsymbol{\sigma}} = \mathbf{D}^{ep}\dot{\boldsymbol{\varepsilon}} \tag{5.39}$$

where, in compliance to previously discussed symmetric properties, it may be noticed that for associated plasticity $\mathbf{D}^{ep} = \mathbf{D}^{ep^T}$ whereas for non-associated plasticity $\mathbf{D}^{ep} \neq \mathbf{D}^{ep^T}$ [28]. To contain the quadratic convergence of the Newton-Raphson iterative solver, the stiffness matrix must account for the algorithmic stress update. The algorithmic tangent stiffness matrix, $\mathbf{D}_{ats}$, first introduced by [29] and [30] is presented in paper B.

5.2 PHASE-FIELD APPROACH FOR BRITTLE FRACTURES IN ROCK

The ability to predict rock behaviour using numerical models is pivotal to solve many rock-engineering problems. Numerical modelling can also be used to improve our understanding of the complicated failure process in rock. With models that better capture the fundamental failure mechanisms observed in laboratory, our ability to generate reliable large-scale models improves. This section presents an alternative method to simulate propagation and nucleation of fractures in rock which uses the variational formulation for quasi-static brittle fracture mechanics first introduced by Francfort and Margio [31]. Early work by Bourdin [32] first introduced a numerical implementation of the regularised approximation of the variational formulation. Following the work by Miehe et al. [33], which gave an interpretation of the phase-field parameter in context of a gradient model, the phase-field fracture model has extended in a number of directions, including dynamic fracture [1–3], coupled thermo-mechanical-driven fracture [4], and high-order phase-field approaches [5], to name a few. However, these contributions assume that the critical energy release rate for different fracture modes are equal, which is not the case for rocks and rock like materials, see, e.g. [6]. In rock-like materials, the critical energy release rate for Mode I and Mode II can differ significantly. In [34] Zhang et al. suggest a model that distinguish between the critical release rates for Mode I and Mode II cracks. However, porous rocks, such as sandstone and volcanic rock, often display fractures due to compressive stresses, see e.g., [15], which is not taken into account in [34].

This section describes the fundamental theory of phase-field fracture models, where a fracture is indicated by a scalar order parameter coupled to the material properties in order to model the change in stiffness between undamaged and broken material. Undamaged material is indicated by that the order parameter has the value one and the material properties remain unaltered, whereas broken material is characterised by the value zero of the order parameter and the stiffness of the material is reduced accordingly. The section continues with a presentation of a modified phase-field fracture model that distinguishes between fractures in Mode I and Mode II as well as fractures driven by compressive stress. The suggested model is capable of capturing the experimental results of rock specimen under plane-strain uniaxial

conditions subjected to compressive loading, see Paper C and Paper D.

5.2.1 Griffith's theory of brittle failure

As a starting point to the phase-field fracture model, a brief recapitulation of the Griffith energy-based failure criterion is given. The criterion is based on linear elastic fracture mechanics and it is set forth that the elastic energy released during fracture propagation is balanced by newly created surface energy. Consider an arbitrary body $\Omega \subset \mathbb{R}^n$, $n \in \{1, 2, 3\}$, with the external boundary $\partial\Omega$ and internal discontinuity boundary Γ, see Figure 5.5a. Griffith's theory of brittle failure states that the total energy of the body is given by

$$\Psi = \Psi_e + \Psi_d - \Psi_{ext} \tag{5.40}$$

where Ψ_e denotes the elastic energy of the undamaged body Ω, Ψ_d the energy needed for evolution of the internal discontinuity $\Gamma(t)$ and Ψ_{ext}, the potential energy of the external forces. If we let ε_{ij} denote the infinitesimal strain tensor, then for the case of linear elasticity, the elastic energy of a body Ω is given by

$$\Psi_e = \int_\Omega \psi_e^0(\varepsilon_{ij})\ dV \tag{5.41}$$

where ψ_e^0 is the undamaged elastic energy density, i.e.,

$$\psi_e^0(\varepsilon_{ij}) = \frac{1}{2}\lambda\varepsilon_{ii}\varepsilon_{jj} + \mu\varepsilon_{ij}\varepsilon_{ji} \tag{5.42}$$

where λ and μ are the Lamé constants. Furthermore, the energy needed for a crack to propagate can be obtained from

$$\Psi_d = \int_\Gamma \mathcal{G}_c\ dA \tag{5.43}$$

where $\mathcal{G}_c$ is the critical strain energy release rate presented in Section 4.2.2. Lastly, the potential energy of the external forces $\Psi_{ext} = 0$ if no external forces are acting on the body.

5.2.2 Phase-field fracture approximation

To avoid the problems associated with numerically tracking the evolution of an internal discontinuity boundary Γ, a phase-field parameter, $d(\boldsymbol{x}, t) \in [0, 1]$ is used to approximate a fracture surface. The material is undamaged as long as the phase-field parameter $d = 1$ and a fracture is represented by $d = 0$, see Figure 5.5b. The foundation of the phase-field fracture model is the approximation of the total

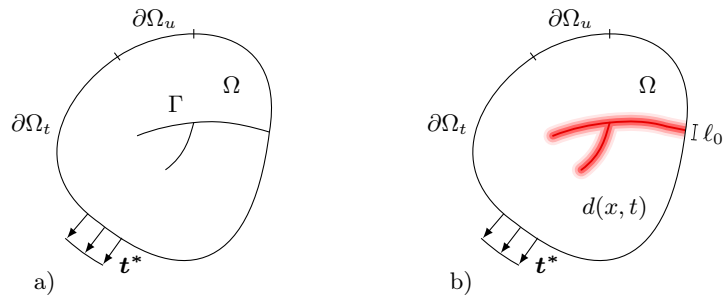

Figure 5.5: a) Representation of a solid body Ω with internal discontinuity boundary Γ. b) Approximation of internal discontinuity boundaries by the phase-field, $d(x,t)$.

energy of a fractured body, equation (5.40). A number of different methods have been suggested to approximate the fracture energy. One widely used formulation was suggested by Miehe et al. [35]. The formulation is thermodynamically consistent and can to some extent be seen as an alternation to the framework of Francfort and Margio [31] and Bourdin [32], where the fracture energy is approximated as

$$\Psi_d = \int_\Gamma \mathcal{G}_d \; dA \;\approx \int_\Omega \psi_d \; dV \tag{5.44}$$

where

$$\psi_d = \mathcal{G}_c \Big[\frac{(d-1)^2}{4\ell_0} + \ell_0 \frac{\partial d}{\partial x_i} \frac{\partial d}{\partial x_i} \Big] \tag{5.45}$$

in which ℓ_0 is a model parameter that controls the width of the approximation of the fracture zone, see Figure 5.5. Borden [36] and Kuhn [37] suggest that the regularised length, ℓ_0, can be regarded as a material parameter, determined as $\ell_0 = \frac{27E\mathcal{G}_c}{512\sigma_t^2}$, where E is the Young's modulus, σ_t the tensile strength and $\mathcal{G}_c$ the critical energy release rate. In [38], Bourdin et al. noticed that the early phase-field approximations gave unrealistic crack patterns during compression. To remedy this problem, Miehe et al. [35] suggested a decomposition of the elastic energy $\psi_e^0(\boldsymbol{u}, d) = \psi(\boldsymbol{\varepsilon})_e^+ + \psi(\boldsymbol{\varepsilon})_e^-$. To model the decrease of material stiffness as the fracture propagates, the elastic energy density is defined as

$$\psi_e^0(\boldsymbol{u}, d) = [(1-\eta)d^2 + \eta]\psi_e^+ + \psi_e^- \tag{5.46}$$

where η is a correction factor to ensure numerical stability, set to approximately $1e^{-12}$. The elastic energy densities are given from:

$$\psi_e^+(\varepsilon) = \frac{1}{2}\lambda\langle\varepsilon_{ii}\rangle^2 + \mu\varepsilon_{ij}^+\varepsilon_{ji}^+ \tag{5.47}$$

$$\psi_e^-(\varepsilon) = \frac{1}{2}\lambda[\varepsilon_{ii} - \langle\varepsilon_{ii}\rangle]^2 + \mu\varepsilon_{ij}^-\varepsilon_{ji}^- \tag{5.48}$$

in which ε^+ and ε^- are the positive and negative components of the strain tensor, i.e.,

$$\begin{aligned} \boldsymbol{\varepsilon}^+ &= \mathbf{P}\boldsymbol{\Lambda}^+\mathbf{P}^T \\ \boldsymbol{\varepsilon}^- &= \mathbf{P}\boldsymbol{\Lambda}^-\mathbf{P}^T \end{aligned} \tag{5.49}$$

with

$$\boldsymbol{\Lambda}^+ = \mathrm{diag}(\langle\lambda_1\rangle, \langle\lambda_2\rangle, \langle\lambda_3\rangle) \qquad \boldsymbol{\Lambda}^- = \boldsymbol{\Lambda} - \boldsymbol{\Lambda}^+ \tag{5.50}$$

and where $\mathbf{P}$ consists of the orthonormal eigenvectors of $\boldsymbol{\varepsilon}$ and $\boldsymbol{\Lambda} = \mathrm{diag}(\lambda_1, \lambda_2, \lambda_3)$ is a diagonal matrix of principal strains, with the Macaulay brackets defined as

$$\langle x\rangle = \begin{cases} x & x \geq 0 \\ 0 & x < 0 \end{cases} \tag{5.51}$$

The stress tensor can now be calculated as the derivative of the elastic strain energy density, given in equation (5.46), as

$$\sigma_{ij} = \partial_\varepsilon \psi_e^0(\boldsymbol{\varepsilon}, d) = [(1-\eta)d^2 + \eta]\Big[\partial_\varepsilon \psi_e^+(\boldsymbol{\varepsilon})\Big] + \partial_\varepsilon \psi_e^-(\boldsymbol{\varepsilon}) \tag{5.52}$$

By adding the expressions according to equation (5.45) and equation (5.46) the total strain energy density of the phase-field approximation can be formulated as,

$$\psi(\varepsilon, d) = [(1-\eta)d^2 + \eta]\psi_e^+ + \psi_e^- + \mathcal{G}_c\left[\frac{(d-1)^2}{4\ell_0} + \ell_0|\nabla d|^2\right] \tag{5.53}$$

Furthermore, the evolution of the phase-field can be determined from

$$\dot{d} = -M\frac{\delta\psi}{\delta d} = -M\left[2d[1-\eta]\psi_e^+ + \frac{\mathcal{G}_c}{2\ell_0}[d-1] + 2\mathcal{G}_c\ell_0\Delta d\right]. \tag{5.54}$$

where the constraint $\dot{d}\frac{\delta\psi}{\delta d} \geq 0$ is introduced to enforce growth of the fracture work Ψ_d in equation (5.44). The kinetic coefficient or mobility parameter M is a non-negative scalar function $M = M(\boldsymbol{\varepsilon}, d, \nabla d, \dot{d})$ introduced to control the crack velocity. The most simple assumption, M = constant lead to the standard Ginzburg-Landau evolution equation, see [37]. Furthermore, the variational derivative of ψ is given by

$$\frac{\delta\psi}{\delta d} = \frac{\partial\psi}{\partial d} - \mathrm{div}\Big(\frac{\partial\psi}{\partial\nabla d}\Big) \qquad \text{with} \qquad \mathrm{div}\Big(\frac{\partial\psi}{\partial\nabla d}\Big) = 2\mathcal{G}_c\ell_0\Delta d \tag{5.55}$$

The split in the elastic strain energy, presented here and suggested by [35], prevents propagation fractures in compression. However, the split of the strain energy leads to a strongly non-linear stress-strain relation, equation (5.52), increasing the computational cost. Moreover, equation (5.54) implies that the critical energy release rates in Mode I and Mode II cracks are equal, which is not the case for most rock.

5.2.3 Modified phase-field approximation

A number of different approaches have been proposed to overcome the limitations of the phase-field fracture models when it comes to simulating materials with different values of critical energy release rates for fractures for Mode I and Mode II. In [39], Choo et al. present an alternative, in which the regularisation length ℓ_0 and the fracture energy density $\mathcal{G}_c$ are chosen such that the peak stress under uni-axial loading matches to the Mohr-Coulomb yield criterion. However, the work presented in this thesis, this limitation of the phase-field fracture is approached with a method inspired by [34] and a modified version of the phase-field model that accommodates for the characteristic behaviours of porous rock is proposed. The goal with the proposed model is to:

- capture the evolution of fractures in porous rock.
- control the critical energy release rates for Mode I and Mode II fractures.
- allow for fractures driven by compressive stress.

To allow for fractures in both compression and tension, a modification of the elastic strain energy density is introduced by redefining equation (5.46) into

$$\psi_e(\boldsymbol{u}, d) = [(1-\eta)d^2 + \eta]\mathcal{H} \tag{5.56}$$

where $\mathcal{H} = \mathcal{H}^+ + \mathcal{H}^-$ is a reformulation of the elastic strain energy density introduced to control the evolution of cracks in both tension and compression, which will be discussed further shortly. First, we focus on how to separate between Mode I and Mode II fractures as the critical energy release rates for rocks, in general are not the same for shear and tensile cracks. In [40], Ambati et al. give an overview of different phase-field fracture formulations, including the approaches proposed by [35, 37, 41] among others. Where [41] suggest that the elastic strain energy should be formulated using a deviatoric and volumetric split,

$$\psi_e^+(\varepsilon) = \frac{1}{2}K_n\langle\varepsilon_{ii}\rangle^2 + \mu\ \varepsilon_{ij}^{dev}\varepsilon_{ji}^{dev} \tag{5.57}$$

$$\psi_e^-(\varepsilon) = \frac{1}{2}K_n[\varepsilon_{ii} - \langle\varepsilon_{ii}\rangle]^2 \tag{5.58}$$

with $K_n = \lambda + \frac{2\mu}{n}$ and ε_{ij}^{dev} the deviatoric strain given as $\varepsilon_{ij}^{dev} = \varepsilon_{ij} - \frac{1}{n}\varepsilon_{kk}\delta_{ij}$ with $n = 2, 3$ representing the dimension of the problem. A benefit with this approach is that it presents a pure split between the volumetric and deviatoric strains, but the formulation leads to cracking in regions where all principal strains are negative, which can have an effect on the crack path. To demonstrate the effects of the different models, 5.2.4, presents a numerical example of single edge notch shear test, where the results presented in Figure 5.7, gives an example of how the crack

path is effected. To overcome this problem, whilst still having a split between the volumetric and deviatoric parts of the strain tensor, a modified formulation of the strain energy terms for the evolution of the phase-field is suggested, defined as

$$\mathcal{H}^{+}(\varepsilon) = \left[\frac{1}{2}K\langle\varepsilon_{ii}\rangle^2 + \mu\ \varepsilon_{ij}^{d+}\varepsilon_{ji}^{d+}\right] H(\varepsilon_{ii}) \tag{5.59}$$

$$\mathcal{H}^{-}(\varepsilon) = \left[\frac{1}{2}K[\varepsilon_{ii} - \langle\varepsilon_{ii}\rangle]^2 + \mu\ \varepsilon_{ij}^{d-}\varepsilon_{ji}^{d-}\right] [1 - H(\varepsilon_{ii})] \tag{5.60}$$

with the tensors $\varepsilon_{ij}^{d+} = \varepsilon_{ij}^{+} - \frac{1}{n}\varepsilon_{kk}\delta_{ij}$ and $\varepsilon_{ij}^{d-} = \varepsilon_{ij}^{-} - \frac{1}{n}\varepsilon_{kk}\delta_{ij}$ and where $H(\varepsilon_{ii})$ the Heaviside function. Next, a new *mobility parameter* is introduced, $\tilde{M} = M\mathcal{G}_c$ by rearranging equation (5.54) into,

$$2d[1-\eta]\frac{\mathcal{H}}{\mathcal{G}_c} + \frac{1}{2\ell_0}[d-1] + 2\ell_0\Delta d + \frac{\dot{d}}{\tilde{M}} = 0, \tag{5.61}$$

where the ratio $\frac{\mathcal{H}}{\mathcal{G}_c}$ controls the evolution of the crack. Porous rocks, e.g., sandstone or volcanic rock, often display fractures during compressive stress, [42]. To overcome this problem, a change to equation (5.61) is proposed, where a modification to the ratio $\frac{\mathcal{H}}{\mathcal{G}_c}$ enables mixed mode crack propagation under both tensile and compressive stress,

$$\frac{\mathcal{H}}{\mathcal{G}_c} = \frac{\mathcal{H}_I^{+}}{\mathcal{G}_{cI}^{+}} + \frac{\mathcal{H}_{II}^{+}}{\mathcal{G}_{cII}^{+}} + \frac{\mathcal{H}_I^{-}}{\mathcal{G}_{cI}^{-}} + \frac{\mathcal{H}_{II}^{-}}{\mathcal{G}_{cII}^{-}} \tag{5.62}$$

with

$$\begin{aligned}
\mathcal{H}_I^{+} &= \frac{1}{2}K\langle\varepsilon_{ii}\rangle^2 H(\varepsilon_{ii}) \\
\mathcal{H}_{II}^{+} &= \mu\ \varepsilon_{ij}^{d+}\varepsilon_{ji}^{d+} H(\varepsilon_{ii}) \\
\mathcal{H}_I^{-} &= \frac{1}{2}K[\varepsilon_{ii} - \langle\varepsilon_{ii}\rangle]^2[1 - H(\varepsilon_{ii})] \\
\mathcal{H}_{II}^{-} &= \mu\ \varepsilon_{ij}^{d-}\varepsilon_{ji}^{d-}[1 - H(\varepsilon_{ii})].
\end{aligned} \tag{5.63}$$

where the parameters $\mathcal{G}_{cI}^{+}$, $\mathcal{G}_{cII}^{+}$ are the critical energy release rates for Mode I and Mode II during tensile stresses and where $\mathcal{G}_{cI}^{-}$ and $\mathcal{G}_{cII}^{-}$ represent the critical energy release rates for compressive stresses. Besides the modification of the ratio $\frac{\mathcal{H}}{\mathcal{G}_c}$ a non-constant mobility parameter $\tilde{M}(\boldsymbol{\varepsilon}) = \tilde{m}_1 + \tilde{m}_2 H(\mathrm{tr}[\boldsymbol{\varepsilon}])$ is proposed to give further control of the evolution.

The performance of the proposed modified phase-field fracture for both nucleation and propagation of fractures in rock under uni-axial compression have been demonstrated in Paper C and Paper D. The work presented in Paper C shows the ability of the proposed model to reproduce experimental results of crack evolution for artificial rock samples with pre-existing inclined cuts. Paper D demonstrates the ability of the model to reproduce crack nucleation without any pre-existing sharp corner.

Finally, it should be noted that, when simulating fractures under compression, the internal surfaces of the crack will in many cases come into contact. Even though the presented phase-field model, do not take this self contact into account the proposed model produces results in good agreement to experimental observations both with respect to crack patterns and critical stress loads.

5.2.4 Numerical simulation of a single edge notched shear test

To demonstrate that the choice made for the strain energies equation (5.59)-(5.60) does not affect the capability of the model to generate fractures driven from only tensile stresses, this section presents the numerical results for a single edge notched shear example, often used as a benchmark within the phase-field fracture community. To demonstrate that, for the special case of $\mathcal{G}_{cI}^{+} = \mathcal{G}_{cII}^{+}$ and $\mathcal{G}_{cIII}^{-} = \mathcal{G}_{cIV}^{-} \approx \infty$, the proposed model produces results in good agreement with [35]. The simulation has been run for the three different formulations, the model proposed by [35], the one proposed by [41] and the model presented in Paper D. The shear test is comprised of a square plate with a single initial crack from the left edge to the middle of the plate along the horizontal centre-line, see Figure 5.6. For the simulation the Young's modulus is $E = 210$ GPa, Poisson's ratio $\nu = 0.3$ and the critical energy release rate $\mathcal{G}_{cI} = \mathcal{G}_{cII} = 2.7 \times 10^{-3}$ MN/m. For the proposed model, the $\mathcal{G}_{cIII}^{+} = \mathcal{G}_{cIV}^{+} = 1 \times 10^{10}$ MN/m, an artificially high value, such that no fractures will evolve from compressive stresses during the simulation. The simulations are conducted using a uniform mesh with element size $h_e = \frac{1}{2}\ell_0$ which coincides with a mesh of approximately $74,000$ elements. Furthermore, the simulations are run using a displacement driven context with constant displacement increment of $\Delta u = 1 \times 10^{-5}$ mm, and the mobility parameter $\tilde{m}_1 = 1.0 \times 10^{-12}$ and $\tilde{m}_1 + \tilde{m}_2 = 1.0$.

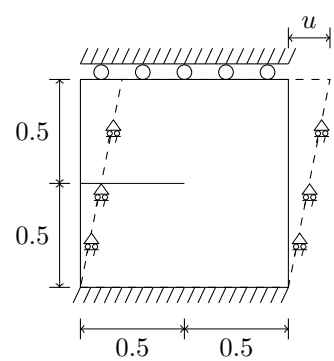

Figure 5.6: Geometry and boundary conditions for the 1×1 mm^2 plate in the single edge notched shear test.

Figure. 5.7 presents the crack pattern at different stages of the simulation while Figure. 5.8 shows the load-deflection curve for the single edge notched test. The results produced with the suggested modified phase-field model are in good agreement with the results presented by Miehe et al. [35] and Amor et al. [41]. Furthermore, in the results from the model proposed by Amor et al. the crack makes a sharp turn toward the right edge of the plate just before reaching the bottom of the plate. In the absence of experimental results, it is difficult to judge which result is more physically relevant, but crack appearing the results from the model proposed by Amor et al. is not seen in the results from the other models.

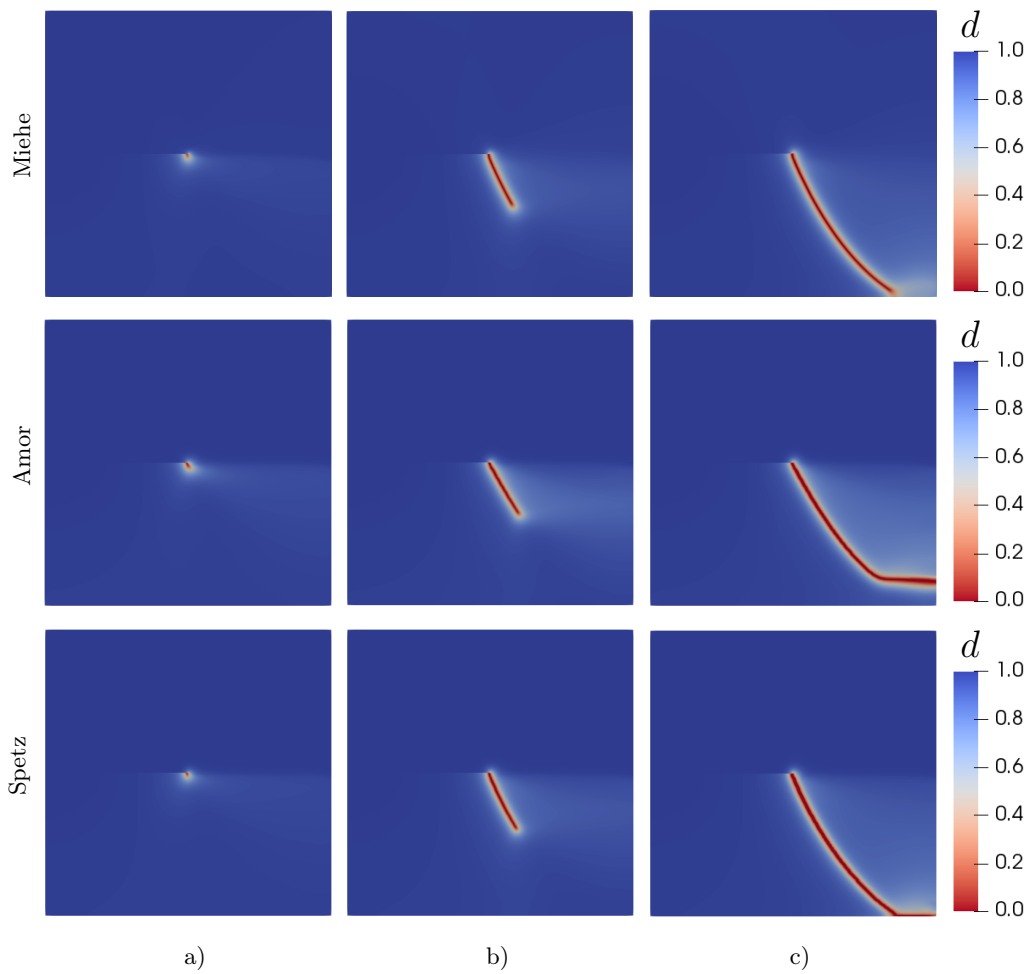

Figure 5.7: Crack patterns for the single edge notched shear test. a) $u = 9.8{\times}10^{-3}$ mm, b) $u = 11.8 \times 10^{-3}$ mm and c) $u = 14.0 \times 10^{-3}$ mm.

The results shown in Figure 5.7 and 5.8 demonstrate that the proposed modified

phase-field fracture model produces negligible changes in the predicted crack path as well as only small differences in the load-deflection curves compared to earlier work using the standard phase-field fracture model.

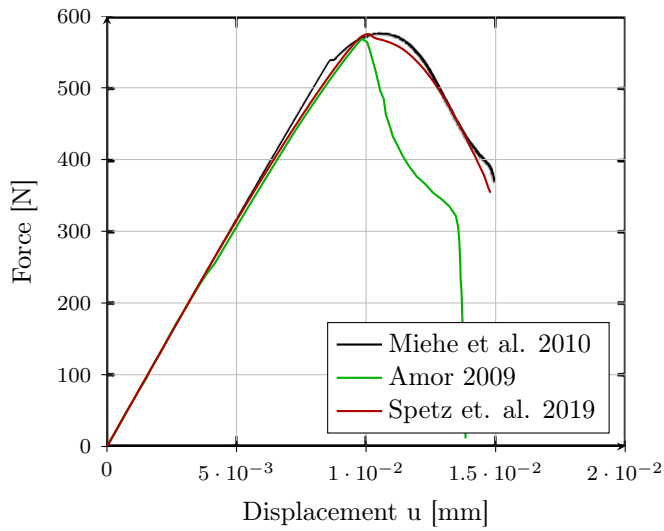

Figure 5.8: Force-displacement curve for the single edge notched shear test.

It can be observed, that even for this special case of $\mathcal{G}_{cI}^{+} = \mathcal{G}_{cII}^{+}$ and $\mathcal{G}_{cI}^{-} = \mathcal{G}_{cII}^{-} \approx \infty$, the proposed model differs from the models presented in earlier work, in the choice made for the strain energies in equation. (5.59) and (5.60). Another benefit of using the model proposed in this thesis is that formulation converges in a significantly lower number of iterations to find the solution of the mechanical part than the models proposed by Miehe et al. [35] and Amor et al. [41]. This is likely due to the redefining equation. (5.46) into equation. (5.56).

5.3 NUMERICAL FORMULATION

5.3.1 Finite element method

The finite element method was introduced to engineering applications in the 1960s, and is a numerical method that solves general differential equations in an approximate manner. This is done by assuming that the differential equation that describes the physical problems holds for a set region. Instead of finding an approximation that holds over the entire region, the region is divided into smaller parts, so-called finite elements, for which the approximation is applied. The assembly of all elements is called a *finite element mesh*. Even if the physical problem varies in a highly

non-linear manner over the region, it is assumed that a linear or quadratic approximation will hold in each element. This is acceptable if the element is small enough. Having found the solution for the individual elements it is possible to find the approximate solution for the entire region. Extensive work have been accomplished on the topic over the years, see, e.g., [43–45] for an overview.

5.3.2 Isogeometric analysis

Hughes et al., [46], first suggested the term isogeometric analysis, as the name for a recently developed computational approach that utilises the design geometry for analysis. Although earlier work has been presented on computational approaches using the original design from Computer Aided Geometric Design (CAGD), the pioneering work by Hughes et al. [46] revealed the potential of using Non-Uniform Rational B-splines for analysis.

The main concept behind the development of isogeometric analysis was that, by using the same basis function for both geometrical and numerical discretisation, it would be possible to reduce the overall computational cost. The idea was that, by going from the use of piecewise polynomials to approximate the geometry and solution fields to utilising the basis functions from CAGD also for analysis, it would be possible to remove the need to recreate a geometry and constructing a mesh for analysis. Even though the original goal, to remove the need to create separate models for analysis, might not have been reached, the use of higher-order basis function has proven to have other benefits, i.e., a smother representation of the solution fields as well as opening up the possibility of using quadrature rules evaluated on element boundaries, reducing the total number of quadrature points [46], [47]. To give a brief introduction to the concept of IGA and to elucidate some of the differences between conventional FEA and IGA, this section will review the basic concepts of isogeometric analysis. For a more extensive description, the reader is referred to [46] and [19].

Basic concept of B-splines

To introduce the concept of the NURBS-based isogeometric framework used in this work we start by defining a B-spline curve. A B-spline curve is a linear combination of B-spline basis functions, $N_{i,p}$, $i = 1, 2, ..., n$ and a set of corresponding control points $\mathbf{P}_i \in \mathbb{R}^d$, $i = 1, 2, ..., n$.

$$\mathbf{C}(\xi) = \sum_{i=1}^{n} N_{i,p}(\xi)\mathbf{P}_i \tag{5.64}$$

An example of a second order B-spline with three control points is illustrated in Figure 5.9. The B-spline basis functions $N_{i,p}$ are constructed from a non-decreasing

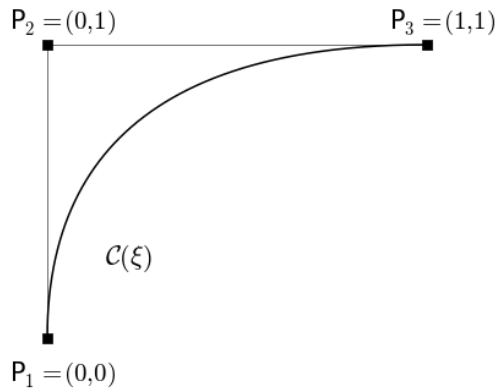

i	$\mathbf{P}_i$
1	(0, 0)
2	(0, 1)
3	(1, 1)

$$\Xi = \{\xi_1, \xi_2, \xi_3, \xi_4, \xi_5, \xi_6, \} = \{0, 0, 0, 1, 1, 1\}$$

Figure 5.9: A second order B-spline curve, $C(\xi)$.

set of coordinates in the parameter space, written as $\Xi = \{\xi_1, \xi_2, ..., \xi_{n+p+1}\}$, where $\xi_i \in \mathbb{R}$ denotes the ith knot of the knot vector Ξ, p indicates the order of the polynomial function and n represents the number of basis functions needed to construct a specific B-spline curve. With a given knot vector, ξ_i, and a known polynomial order, p, it is possible to construct a B-spline basis function. For the case of $(p = 0)$, the basis function takes a piecewise constant shape given from

$$N_{i,0}(\xi) = \begin{cases} 1 & \text{if } \xi_i \leq \xi < \xi_{i+1} \\ 0 & \text{otherwise} \end{cases} \tag{5.65}$$

For $p = 1, 2, 3, ...$ the B-spline basis function can be constructed by using the expression,

$$N_{i,p}(\xi) = \frac{\xi - \xi_i}{\xi_{i+p} - \xi_i} N_{i,p-1}(\xi) + \frac{\xi_{i+p+1} - \xi}{\xi_{i+p+1} - \xi_{i+1}} N_{i+1,p-1}(\xi) \tag{5.66}$$

which is referred to as the Cox-de Boor formula, first presented in [48] and [49].

NURBS representation

One issue arising when using B-spline, is that not all types of geometries can be represented exactly using polynomial functions. To overcome this problem rational B-splines were introduced by Versprille in [50]. This generalisation of B-splines is constructed by introducing a non-negative weight, w_i, to each control point and making use of the definition of *rational functions* as the ratio of two polynomials [51]. Non-Uniform Rational B-splines or NURBS are today standard in many CAGD softwares and the fact that NURBS algorithms are fast and stable make them a good choice also for analysis. To construct NURBS basis functions one can make

use of the basis functions for B-splines,

$$R_i^p(\xi) = \frac{N_{i,p}(\xi) w_i}{W(\xi)} \tag{5.67}$$

where $W(\xi)$ is called a weighting function, defined as

$$W(\xi) = \sum_{\hat{i}=1}^{n} N_{\hat{i},p}(\xi) w_{\hat{i}} \tag{5.68}$$

If $w_i = 1$ for all i, then $R_i^p(\xi) = N_{i,p}(\xi)$ for all i. In fact, if the value of $w_i = a$ for all i then $R_i^p(\xi) = N_{i,p}(\xi)$, i.e., the $N_{i,p}(\xi)$ are special cases of $R_i^p(\xi)$ where all the weights take the same value. Using the NURBS basis functions $R_i^p(\xi),\ i = 1, 2, ..., n$ and their corresponding control points $\mathbf{P}_i$, a piecewise NURBS curve, is constructed from

$$\mathbf{C}(\xi) = \sum_{i=1}^{n} R_i^p(\xi) \mathbf{P}_i \tag{5.69}$$

To be able to perform two- and three-dimensional analysis, NURBS surfaces and bodies need to be defined. This is done in a similar manner. A NURBS body is given by

$$\mathbf{S}(\xi, \eta, \zeta) = \sum_{i=1}^{n} \sum_{j=1}^{m} \sum_{k=1}^{l} R_{i,j,k}^{p,q,r}(\xi, \eta, \zeta) \mathbf{P}_{i,j,k} \tag{5.70}$$

where the NURBS basis function, $R_{i,j,k}^{p,q,r}(\xi, \eta, \zeta)$, is constructed from three sets of knot vectors, and their respective weighting functions $W(\xi, \eta, \zeta)$.

$$R_{i,j,k}^{p,q,r}(\xi, \eta, \zeta) = \frac{N_{i,p}(\xi) M_{j,q}(\eta) L_{k,r}(\zeta) w_{i,j,k}}{W(\xi, \eta, \zeta)} \tag{5.71}$$

where

$$W(\xi, \eta, \zeta) = \sum_{\hat{i}=1}^{n} \sum_{\hat{j}=1}^{m} \sum_{\hat{k}=1}^{l} N_{\hat{i},p}(\xi) M_{\hat{j},q}(\eta) L_{\hat{k},r}(\zeta) w_{\hat{i},\hat{j},\hat{k}} \tag{5.72}$$

In the isogeometric framework the concept of elements is represented by the non-zero valued knot spans. This is illustrated in Figure 5.10, where a two dimensional plate is constructed from two knot vectors, a set of control points $\mathbf{P}_{i,j}$ and their corresponding weights $w_{i,j}$. The geometry is constructed of one knot vector, $\Xi = \{0, 0, 0, 0.5, 1, 1, 1\}$ in the direction of the arc of the hole and one knot vector, $\mathcal{H} = \{0, 0, 0, 1, 1, 1\}$, in the radial direction, thus creating a plate consisting of two elements. The element specific basis functions are constructed from the non-zero valued basis functions in the active knot span. The number of active functions in a knot span is determined as $n_p = (p + 1) \times (q + 1) \times (r + 1)$. For analysis, the basis functions are evaluated at the chosen integration points of the parent element, see Figure 5.10d). These element specific NURBS basis functions will be denoted $N_a^e(\xi, \eta, \zeta)$ in the remainder of this work.

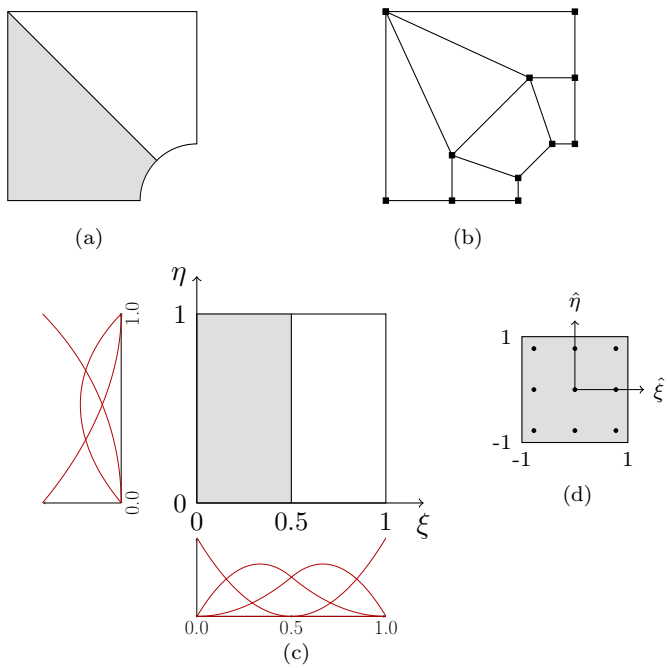

i	j	$\mathbf{P}_{i,j}$	$w_{i,j}$
1	1	(-4, 0)	1.0
1	2	(-2.5, 0)	1.0
1	3	(-1, 0)	1.0
2	1	(-4, 4)	1.0
2	2	(-2.5, 0.83)	1.0
2	3	(-1, 0.41)	$(1+\frac{1}{\sqrt{2}})/2$
3	1	(-4, 4)	1.0
3	2	(-0.83, 2.5)	1.0
3	3	(-0.41, 1)	$(1+\frac{1}{\sqrt{2}})/2$
4	1	(0, 4)	1.0
4	2	(0, 2.5)	1.0
4	3	(0, 1)	1.0

$$\Xi = \{\xi_1, \xi_2, \xi_3, \xi_4, \xi_5, \xi_6, \xi_7\} = \{0, 0, 0, 0.5, 1, 1, 1\}$$

$$\mathcal{H} = \{\eta_1, \eta_2, \eta_3, \eta_4, \eta_5, \eta_6\} = \{0, 0, 0, 1, 1, 1\}$$

Figure 5.10: A NURBS surface of the symmetric part of a plate with a circular hole constructed from two knot vectors, Ξ and $\mathcal{H}$, a set of control points, $\mathbf{P}_{i,j}$ and their corresponding weights, $w_{i,j}$. a) shows the element mesh b) the control net c) the parameter space and basis functions d) the parent element.

Note that the physical implication on the curve from duplicating a knot value is that a sharp corner is created at $\xi = 2$. The reduced continuity at duplicated knot values also has implications for analysis. The possibility to govern the continuity of the basis functions also allows the determination of the continuity of the stresses solved for in a displacement-based analysis. This can be used, e.g., to define material boundaries.

Discretisation

The main difference between conventional FEA and IGA are the basis functions used for discretisation. In isogeometric analysis the same basis functions that are used to discretise the geometry are also used to solve for the approximate displacement solution fields. The only difference to conventional FEA is that the basis functions in IGA are element-specific. After solving the element-specific basis functions and

their derivatives the procedure of establishing the stiffness matrix and internal force vector is identical to conventional FEA. The displacement field for any given element can be solved using the element specific basis function $N_a^e(\xi, \eta, \zeta)$,

$$\mathbf{u} = \sum_{a=1}^{n_p} N_a^e(\xi, \eta, \zeta)\mathbf{a}_a^e \tag{5.73}$$

with $\mathbf{a}_a^e$ the element displacements. The discretised form of the crack field is given from

$$d = \sum_{a=1}^{n_p} N_a^e(\xi, \eta, \zeta) d_{h\ a}^e \tag{5.74}$$

The spatial derivatives of the displacement field can be approximated by taking the derivative of the element-specific basis functions with respect to the physical coordinates $\mathbf{x}$,

$$\nabla\mathbf{u} = \sum_{a=1}^{n_p} \frac{\partial N_a^e}{\partial \mathbf{x}}\mathbf{a}_a^e \tag{5.75}$$

similarly, the derivatives of the phase-field can be approximated by

$$\nabla d = \sum_{a=1}^{n_p} \frac{\partial N_a^e}{\partial \mathbf{x}} d_{a\ h}^e \tag{5.76}$$

To obtain the derivatives of the basis functions with respect to the physical coordinates, one must use the chain rule,

$$\frac{\partial N_a^e}{\partial \mathbf{x}} = \frac{\partial N_a^e}{\partial \boldsymbol{\xi}} \frac{\partial \boldsymbol{\xi}}{\partial \mathbf{x}} \tag{5.77}$$

with $\boldsymbol{\xi} = \{\xi, \eta, \zeta\}^T$. For a more straightforward implementation we rewrite the displacement field using a vector-matrix notation, i.e., $\mathbf{u} = \mathbf{N}^e\mathbf{a}^e$, where the matrix $\mathbf{N}^e$ contains the basis functions $N_a^e(\xi, \eta, \zeta)$ for each control point in support of an element

$$\mathbf{N}^e = \begin{bmatrix} N_1^e & 0 & 0 & \dots & N_{n_p}^e & 0 & 0 \\ 0 & N_1^e & 0 & \dots & 0 & N_{n_p}^e & 0 \\ 0 & 0 & N_1^e & \dots & 0 & 0 & N_{n_p}^e \end{bmatrix} \tag{5.78}$$

Likewise, the discretised form of the phase-field can be determined as, $d = \mathbf{N}_d^e d_h^e$ with $\mathbf{N}_d^e$ defined as

$$\mathbf{N}_d^e = \begin{bmatrix} N_1^e & N_2^e & \dots & N_n^e \end{bmatrix} \tag{5.79}$$

In a similar manner we rewrite (5.75) in matrix form,

$$\boldsymbol{\varepsilon} = \mathbf{B}^e\mathbf{a}^e \tag{5.80}$$

where the matrix $\mathbf{B}^e$ is an operator mapping the element discrete displacements to the local strains.

$$\mathbf{B} = \begin{bmatrix} \frac{\partial N_1^e}{\partial x_1} & 0 & 0 & \dots & \frac{\partial N_{n_p}^e}{\partial x_1} & 0 & 0 \\ 0 & \frac{\partial N_1^e}{\partial x_2} & 0 & \dots & 0 & \frac{\partial N_{n_p}^e}{\partial x_2} & 0 \\ 0 & 0 & \frac{\partial N_1^e}{\partial x_3} & \dots & 0 & 0 & \frac{\partial N_{n_p}^e}{\partial x_3} \\ \frac{\partial N_1^e}{\partial x_2} & \frac{\partial N_1^e}{\partial x_1} & 0 & \dots & \frac{\partial N_{n_p}^e}{\partial x_2} & \frac{\partial N_{n_p}^e}{\partial x_1} & 0 \\ \frac{\partial N_1^e}{\partial x_3} & 0 & \frac{\partial N_1^e}{\partial x_1} & \dots & \frac{\partial N_{n_p}^e}{\partial x_3} & 0 & \frac{\partial N_{n_p}^e}{\partial x_1} \\ 0 & \frac{\partial N_1^e}{\partial x_3} & \frac{\partial N_1^e}{\partial x_2} & \dots & 0 & \frac{\partial N_{n_p}^e}{\partial x_3} & \frac{\partial N_{n_p}^e}{\partial x_2} \end{bmatrix} \tag{5.81}$$

Finally, the discretised gradient of the fracture field are determined as

$$\nabla d^e = \boldsymbol{B}_d^e d_h^e \tag{5.82}$$

with

$$\mathbf{B}_d^e = \begin{bmatrix} \frac{\partial N_1^e}{\partial x_1} & \frac{\partial N_2^e}{\partial x_1} & \dots & \frac{\partial N_n^e}{\partial x_1} \\ \frac{\partial N_1^e}{\partial x_2} & \frac{\partial N_2^e}{\partial x_2} & \dots & \frac{\partial N_n^e}{\partial x_2} \\ \frac{\partial N_1^e}{\partial x_3} & \frac{\partial N_2^e}{\partial x_3} & \dots & \frac{\partial N_n^e}{\partial x_3} \end{bmatrix} \tag{5.83}$$

The numerical implementation of the presented equations has been used in the work presented in Paper B-D.

6 Conclusions

The use of numerical methods is becoming common practise within geotechnical engineering, and the ability to predict soil and rock behaviour using numerical models is pivotal to solve many engineering problems. In this thesis, research concerning methods for simulating the behaviour of soil and rock behaviour have been presented. The research presented in the dissertation demonstrates both the importance of understanding numerical tools to produce reliable results, as well as the opportunities they offer to increase our understanding of complicated failure processes in rocks and soils.

6.1 MAIN CONTRIBUTIONS

The main contributions of this work include:

- Although numerical methods can be a great help during the design of rather uncomplicated foundations, the use of simplified methods can lead to misconceptions of structural behaviour. This is demonstrated by comparing the effects of using simplified methods to fully coupled finite element analysis during the dimensioning of reinforcements in raft foundations.
- In this thesis, a modified phase-field fracture model for simulation of crack propagation in porous rocks has been proposed. By introducing a split of the fracture energy release rate the proposed phase-field model is able to capture the characteristic behaviour of fractures in porous rock.
- By comparing numerical results to Digital Image Correlation (DIC) analysis carried out during uniaxial plane strain compression tests, Paper C and Paper D have shown that the modified phase-field fracture model gives results in good agreement with the experimental observations both with respect to crack patterns and critical stress loads. It has also been shown that the proposed phase-field model is able to reproduce the formation of compressive

cracks as well as complex crack patterns without any additional algorithmic treatment.

During the course of the research presented in this thesis, it has been shown, that for drained soils, the isogeometric framework is a viable option for modelling of soil behaviour. The use of IGA opens up a new potential for simulations of complicated geotechnical applications. Such as retaining walls in weak soil or installations of friction piles, often involving complicated contact problems and fluid flow, which could benefit from the higher order shape functions of the isogeometric framework.

6.2 FUTURE WORK

The promising results using isogeometric analysis in different engineering fields have the potential to be transferred to soil mechanics and geotechnical engineering. As a number of papers have been published, showing promising results of using isogeometric analysis for flow problems in porous media, a natural step is to expand the analysis presented in Paper B to include steady-state groundwater flow. Another exiting prospect for future work is to apply the isogeometric framework to soil-structure interaction. The C^0-continuous basis function of IGA have a promising outlook on overcome the convergence problem often occurring when using conventional FEA.

Paper C and Paper D have demonstrated that phase-field fracture models have a great potential for simulating complicated fracture processes in rocks. However, one remaining issue for simulations of fractures under compression using any phase-field model is the treatment of self contact of the fracture surfaces. The problem with self contact when using phase-field models provides an interesting challenge to be solved.

References

[1] Tanné, E., Li, T., Bourdin, B., Marigo, J.J., Maurini, C. (2018), *Crack nucleation in variational phase-field models of brittle fracture*, Journal of the Mechanics and Physics of Solids **110**, 80–99.

[2] Schlüter, A., Willenbücher, A., Kuhn, C., Müller, R. (2014), *Phase field approximation of dynamic brittle fracture*, Computational Mechanics **54**(5), 1141–1161.

[3] Carlsson, J., Isaksson, P. (2018), *Dynamic crack propagation in wood fibre composites analysed by high speed photography and a dynamic phase field model*, International Journal of Solids and Structures **144-145**, 78–85.

[4] Hesch, C., Weinberg, K. (2014), *Thermodynamically consistent algorithms for a finite-deformation phase-field approach to fracture*, International Journal for Numerical Methods in Engineering **99**(12), 906–924.

[5] Weinberg, K., Hesch, C. (2017), *A high-order finite deformation phase-field approach to fracture*, Continuum Mechanics and Thermodynamics **29**(4), 935–945.

[6] Shen, B., Stephansson, O. (1994), *Modification of the G-criterion for crack propagation subjected to compression*, Engineering Fracture Mechanics **47**(2), 177–189.

[7] Blaauwendraad, J. (ed.) (2010), *Plates and FEM - Surprises and Pitfalls, Solid Mechanics and its Applications*, vol. 171, Springer.

[8] Kurrer, K.E. (2014), *The History of Theoretical, Material and Computational Mechanics–Mathematics meets Mechanics and Engineering. From E. Stein (ed.)*.

[9] Goldscheider, M. (1984), *True triaxial tests on dense sand*, in: *International workshop on constitutive relations for soils*, 11–54.

[10] Drucker, D.C., Prager, W. (1952), *Soil mechanics and plastic analysis or limit design*, Quarterly of applied mathematics **10**.

[11] Roscoe, K.H. (1970), *The influence of strains in soil mechanics*, Geotechnique **20**(2), 129–170.

[12] Roscoe, K.H., Schofield, A., Wroth, C. (1958), *On the yielding of soils*, Geotechnique **8**(1), 22–53.

[13] Roscoe, K., Burland, J. (1968), *On the generalized stress-strain behaviour of wet clay* .

[14] Yu, H. (1998), *CASM: A unified state parameter model for clay and sand*, International Journal for Numerical and Analytical Methods in Geomechanics **22**(8), 621–653.

[15] Jaeger, J.C., Cook, N.G., Zimmerman, R. (2009), *Fundamentals of rock mechanics*, John Wiley & Sons.

[16] Bond, A., Schuppener, B., Scarpelli, G., Orr, T. (2013), *Eurocode 7: Geotechnical Design. Worked examples*, Publications Office of the European Union.

[17] Desai, C.S., Zaman, M. (2013), *Advanced geotechnical engineering: Soil-structure interaction using computer and material models*, CRC Press.

[18] Winkler, E. (1867), *Theory of elasticity and strength*, Dominicus Prague, Czechoslovakia .

[19] Cottrell, J.A., Hughes, T.J., Bazilevs, Y. (2009), *Isogeometric analysis: toward integration of CAD and FEA*, Wiley, Chichester, West Sussex, U.K., ISBN 9780470748732 (cloth).

[20] Irzal, F., Remmers, J.J., Verhoosel, C.V., Borst, R. (2013), *Isogeometric finite element analysis of poroelasticity*, International Journal for Numerical and Analytical Methods in Geomechanics **37**(12), 1891–1907.

[21] Nguyen, M.N., Bui, T.Q., Yu, T., Hirose, S. (2014), *Isogeometric analysis for unsaturated flow problems*, Computers and Geotechnics **62**, 257–267.

[22] Mitchell, J.K., Soga, K., et al. (2005), *Fundamentals of soil behavior*, vol. 3, John Wiley & Sons Hoboken, NJ.

[23] Terzaghi, K. (1943), *Theory of Consolidation*, Wiley Online Library.

[24] Irwin, G.R. (1957), *Analysis of stresses and strains near the end of a crack traversing a plate*, Journal of Applied Mechanics **6**, 551–590.

[25] Orowan, E. (1949), *Fracture and strength of solids*, Reports on progress in physics **12**(1), 185.

[26] Atkinson, B.K., Meredith, P.G. (1987), *The theory of subcritical crack growth with applications to minerals and rocks*, Fracture mechanics of rock **2**, 111–166.

[27] Desai, C.S., Siriwardane, H.J. (1984), *Constitutive laws for engineering materials with emphasis on geologic materials*, Prentice-Hall.

[28] Ottosen, N.S., Ristinmaa, M. (2005), *The mechanics of constitutive modeling*, Elsevier.

[29] Nagtegaal, J.C. (1982), *On the implementation of inelastic constitutive equations with special reference to large deformation problems*, Computer Methods in Applied Mechanics and Engineering **33**(1), 469–484.

[30] Runesson, K., Booker, J. (1982), *On mixed and displacement finite element methods in perfect elasto-plasticity*, in: *Proceedings of the 4th International Conference in Australia on Finite Element Methods in Engineering.*

[31] Francfort, G.A., Marigo, J.J. (1998), *Revisiting brittle fracture as an energy minimization problem*, Journal of the Mechanics and Physics of Solids **46**(8), 1319–1342.

[32] Bourdin, B. (2007), *Numerical implementation of the variational formulation for quasi-static brittle fracture*, Interfaces and Free Boundaries **9**(3), 411–430.

[33] Miehe, C., Welschinger, F., Hofacker, M. (2010), *Thermodynamically consistent phase-field models of fracture: Variational principles and multi-field FE implementations*, International Journal for Numerical Methods in Engineering **83**(10), 1273–1311.

[34] Zhang, X., Sloan, S.W., Vignes, C., Sheng, D. (2017), *A modification of the phase-field model for mixed mode crack propagation in rock-like materials*, Computer Methods in Applied Mechanics and Engineering **322**, 123–136.

[35] Miehe, C., Hofacker, M., Welschinger, F. (2010), *A phase field model for rate-independent crack propagation: Robust algorithmic implementation based on operator splits*, Computer Methods in Applied Mechanics and Engineering **199**(45-48), 2765–2778.

[36] Borden, M.J., Verhoosel, C.V., Scott, M.A., Hughes, T.J., Landis, C.M. (2012), *A phase-field description of dynamic brittle fracture*, Computer Methods in Applied Mechanics and Engineering **217**, 77–95.

[37] Kuhn, C., Müller, R. (2010), *A continuum phase field model for fracture*, Engineering Fracture Mechanics **77**(18), 3625–3634.

[38] Bourdin, B., Francfort, G.A., Marigo, J.J. (2000), *Numerical experiments in revisited brittle fracture*, Journal of the Mechanics and Physics of Solids **48**(4), 797–826.

[39] Choo, J., Sun, W. (2018), *Coupled phase-field and plasticity modeling of geological materials: From brittle fracture to ductile flow*, Computer Methods in Applied Mechanics and Engineering **330**, 1–32.

[40] Ambati, M., Gerasimov, T., De Lorenzis, L. (2015), *A review on phase-field models of brittle fracture and a new fast hybrid formulation*, Computational Mechanics **55**(2), 383–405.

[41] Amor, H., Marigo, J.J., Maurini, C. (2009), *Regularized formulation of the variational brittle fracture with unilateral contact: Numerical experiments*, Journal of the Mechanics and Physics of Solids **57**(8), 1209–1229.

[42] Vajdova, V., Wong, T.F. (2003), *Incremental propagation of discrete compaction bands: acoustic emission and microstructural observations on circumferentially notched samples of Bentheim*, Geophysical Research Letters **30**(14), 1–8.

[43] Hughes, T.J.R. (2012), *The finite element method: linear static and dynamic finite element analysis*, Courier Corporation.

[44] Bathe, K.J. (1996), *Finite element procedures*, Prentice Hall, Englewood Cliffs, N.J., ISBN 0133014584.

[45] Zienkiewicz, O.C., Taylor, R.L., Zhu, J.Z., *The finite element method: its basis and fundamentals*, seventh edition edn., ISBN 9781856176330 (hardback).

[46] Hughes, T.J.R., Cottrell, J.A., Bazilevs, Y. (2005), *Isogeometric analysis: CAD, finite elements, NURBS, exact geometry and mesh refinement*, Computer Methods in Applied Mechanics and Engineering **194**(39), 4135–4195.

[47] Schillinger, D., Evans, J.A., Reali, A., Scott, M.A., Hughes, T.J. (2013), *Isogeometric collocation: Cost comparison with Galerkin methods and extension to adaptive hierarchical NURBS discretizations*, Computer Methods in Applied Mechanics and Engineering **267**, 170–232.

[48] Cox, M.G. (1972), *The Numerical Evaluation of B-Splines*, IMA Journal of Applied Mathematics **10**(2), 134–149.

[49] de Boor, C. (1972), *On Calculating with B-splines*, Journal of Approximation Theory **6**, 50–62.

[50] Versprille, K.J. (1975), *Computer-aided design applications of the rational B-spline approximation form* .

[51] Piegl, L.A., Tiller, W. (1995), *The NURBS book*, Monographs in visual communication, Springer, ISBN 978-3-540-55069-3.

Part II

Appended publications